PHYSICAL REVIEW D VOLUME 35, NUMBER 5 1 MARCH 1987

Gauginos as a signal for supersymmetry at $p\bar{p}$ colliders

Howard Baer
High Energy Physics Division, Argonne National Laboratory, Argonne, Illinois 60439

Kaoru Hagiwara
Theory Group, KEK, Tsukuba, Ibaraki 305, Japan

Xerxes Tata
Physics Department, University of Wisconsin, Madison, Wisconsin 53706
(Received 15 September 1986)

We present a comprehensive analysis of the signals from the pair production of the mass eigenstates ($\widetilde{W}$, $\widetilde{Z}$, and $\widetilde{\gamma}$) of the gauge-Higgs-fermion system for both CERN and Fermilab Tevatron energies, assuming that $\widetilde{\gamma}$ is relatively light ($\lesssim 10$ GeV) and escapes detection. The effect of varying the mixings and the mass spectrum of the scalar fermions is also discussed for a general minimal supersymmetry model, assuming only that $\widetilde{\gamma}$ is light. Signals from both the hadronic and leptonic decays of $\widetilde{W}$ and $\widetilde{Z}$ are studied, incorporating cuts, triggers, and experimental resolutions appropriate to the UA1 detector and Collider Detector at Fermilab. We show that if the decays $W \rightarrow \widetilde{W}\widetilde{Z}$ and $Z^0 \rightarrow \widetilde{W}\overline{\widetilde{W}}$ are kinematically accessible, there is a substantial level of (i) jet(s) + $\not{p}_T$ events from the hadronic decays of $\widetilde{W}$ and $\widetilde{Z}$, (ii) a comparable level of background-free multilepton + $\not{p}_T$ events, essentially free from hadronic activity from the leptonic decay of $\widetilde{W}$ and $\widetilde{Z}$, and (iii) jet(s) + lepton(s) + $\not{p}_T$ events from the leptonic decay of one of the gauginos and hadronic decay of the other. We present rates and distributions for these events and show that a conclusive absence of such a signal could lead to more stringent direct mass limits on masses of the $\widetilde{W}$ and $\widetilde{Z}$ than are currently available. Absence of multilepton signals implies $m_{\widetilde{W}} \gtrsim 36$–$38$ GeV, corresponding to $m_{\widetilde{Z}} \gtrsim 42$–$44$ GeV, whereas the recently announced UA1 limit on the sequential-heavy-lepton mass translates to $m_{\widetilde{W}} \gtrsim 40$–$44$ GeV, corresponding to $m_{\widetilde{Z}} \gtrsim 45$–$50$ GeV. We have also studied the signals from the decays of $\widetilde{W}$ produced in association with $\widetilde{\gamma}$. Although we find a substantial rate for jet(s) + $\not{p}_T$ events, conclusions based on this signal would entail a study of the substantial standard-model backgrounds. We also conclude that the single lepton + $\not{p}_T$ signal from the leptonic decay of $\widetilde{W}$ would be very difficult to separate from the standard-model background from $W \rightarrow l\bar{\nu}$ and $W \rightarrow l\bar{\nu}\bar{\nu}\nu$.

I. INTRODUCTION

Although the standard $SU(3)\times SU(2)\times U(1)$ model of strong and electroweak interactions describes successfully all the known experimental data, it leaves many fundamental parameters unexplained, such as the ratio of gauge coupling strengths, quark and lepton masses, the number of quark-lepton generalizations, and intergeneration mixing parameters. One of the most attractive ideas toward a theory beyond the standard model is grand unification[1] where the relative strengths of strong, electromagnetic, and weak interactions are explained in terms of a unique coupling and the existence of a large mass gap,[2] or desert, between the standard-model mass scale ($\sim 10^2$ GeV) and the unification mass scale ($\gtrsim 10^{15}$ GeV). It is generally believed that the idea of grand unification can be realized naturally,[3] simply, and phenomenologically consistently only with the help of an extra symmetry, supersymmetry,[4] which interrelates particles with different spins.

Supersymmetry (SUSY) should be broken since we do not observe multiplets with different spin particles. Moreover, in order for supersymmetry to be a solution to the naturalness problem of grand unified theories, all the superpartners of the standard-model particles should have masses below ~ 1 TeV. This is the region to be explored by the present and planned colliders of the near future. Since supersymmetry may open a window towards the unification of all known forces including gravity,[5,6] the experimental searches for superpartners have become and will continue to be one of the most important tasks of high-energy experiments.[7]

Various searches for SUSY particles to date have yielded only negative results. Electron-positron collider experiments set the cleanest limits on SUSY-particle masses.[8] Since these are produced in pairs, direct limits on their masses are typically equal to the beam energy ($\lesssim 23$ GeV). An exception to this is the limit on the Z-gaugino ($\widetilde{Z}$) mass obtained by studying the reaction $e^+e^- \rightarrow \widetilde{Z}\widetilde{\gamma}$, which yields $m_{\widetilde{Z}} \gtrsim 25$–$30$ GeV for $m_{\widetilde{\gamma}} \simeq 0$ and $m_{\widetilde{e}} \lesssim 50$ GeV (Ref. 9). In addition, there are indirect limits such as the limit on the scalar-electron mass (≈ 66 GeV for $m_{\tilde{\gamma}}=0$) obtained by the ASP experiment.[10]

Furthermore, an absence of new physics signals beyond the standard model at the CERN $p\bar{p}$ collider should also lead to bounds on SUSY-particle masses. For example, a conclusive absence of a large number of missing-p_T ($\not{p}_T$) events[11] can be interpreted[12] as lower bounds on scalar-quark and gluino masses, $m_{\tilde{q}} \gtrsim 65-75$ GeV ($m_{\tilde{g}} \gtrsim 60-70$ GeV) depending on $m_{\tilde{g}}$ ($m_{\tilde{q}}$), with a possible exception of a light ($\sim 3-5$ GeV) gluino.[13,14] Leptonic signals from supersymmetry at hadron colliders have also been studied for the cases of light scalar leptons,[15] gaugino decays to scalar leptons,[16] and from the production of strongly interacting SUSY particles.[17]

At this point it is worth noting that in the simplest supergravity models,[18,19] where the breaking of the electroweak symmetry $SU(2)_L \times U(1)$ is induced by the breaking of supersymmetry via gravitational interactions, the scalar masses are typically excepted to be ~ 100 GeV. Furthermore, in the supergravity models with $m_{\tilde{\gamma}} \ll M_W$, there are mass eigenstates $\tilde{W}$ and $\tilde{Z}$ in the gauge-Higgs-fermion sector that have the same internal quantum numbers as the W and Z bosons, but are lighter than the corresponding gauge boson.[20] Since the photino is the cosmologically favored candidate for the lightest supersymmetric particle,[21] this scenario provides us with one of the most attractive possibilities for SUSY-particle spectroscopy. If indeed the superpartners of quarks and leptons are as heavy as or even heavier than 100 GeV, then the signature for supersymmetry most easily accessible in the near future may well come from the weak-boson decays into gaugino pairs:[20,22]

$$W \to \tilde{W}\tilde{\gamma}, \tilde{W}\tilde{Z}, \quad Z \to \tilde{W}\bar{\tilde{W}} . \tag{1.1}$$

The produced W gauginos ($\tilde{W}$'s) and $\tilde{Z}$'s subsequently decay via the processes

$$\tilde{W} \to l\bar{\nu}\tilde{\gamma} \quad \text{or } q\bar{q}'\tilde{\gamma} , \tag{1.2a}$$

$$\tilde{Z} \to l\bar{l}\tilde{\gamma} \quad \text{or } q\bar{q}\tilde{\gamma} . \tag{1.2b}$$

This leads to characteristic n jets + m leptons + $\not{p}_T$ signatures. Purely leptonic signals resulting from these decays at the CERN collider have been studied in Ref. 16 under the condition that scalar leptons are lighter than $\tilde{W}$ and $\tilde{Z}$, i.e., when the gauginos decay via cascade processes:

$$\begin{aligned} &\tilde{W} \to \tilde{l}\bar{\nu}, \quad \tilde{l} \to l\tilde{\gamma} ; \\ &\tilde{Z} \to \tilde{l}\,\bar{l}, \quad \tilde{l} \to l\tilde{\gamma} . \end{aligned} \tag{1.3}$$

Monojet signals from the decays (1.1) have been studied by Chamseddine, Nath, and Arnowitt.[23] In a recent Letter,[24] we reported the results of our survey of all n jet + m leptons + $\not{p}_T$ signals measurable at the CERN $p\bar{p}$ collider.

In this paper, we expand on previous work[24] by including the details of the supergravity model with $m_{\tilde{\gamma}} \ll M_W$ and the presentation of all the relevant amplitudes. Furthermore, the sensitivity of our results to large variation of scalar-fermion masses is examined for the light-photino case and the consequences of the scenario where the scalar neutrino becomes light ($\lesssim m_{\tilde{W}}$) are also studied. Numerical results are given for both CERN and Fermilab Tevatron collider energies.

In the majority of our analysis we have studied the case when the vacuum expectation values of the two Higgs fields that occur in all supersymmetric models are approximately equal ($v=v'$), the scenario favored by many supergravity models.[18,19] Our results are insensitive to scalar-quark and scalar-lepton masses ($\gtrsim 100$ GeV) as far as these are approximately degenerate. When these masses become very high ($m_{\tilde{q}} \simeq m_{\tilde{l}} \gtrsim 350$ GeV), the decay mode

$$\tilde{Z} \to q\bar{q}'\tilde{W} \quad \text{or } l\bar{\nu}\tilde{W} \tag{1.4}$$

starts dominating the decay modes (1.2b). The $\tilde{W}$ would still decay via the usual modes (1.2a). In such cases only the $\tilde{W}\tilde{Z}$ signal would be somewhat modified.

Once we drop the condition $v \simeq v'$, then the approximate degeneracy of scalar-quark and scalar-lepton masses is no longer true and indeed scalar neutrinos can become quite light in the renormalization-group studies[25] starting from a common scalar mass at the unification scale. The decay pattern of $\tilde{W}$'s and $\tilde{Z}$'s changes drastically when the scalar-neutrino mass becomes lighter than the gaugino masses; the decay modes

$$\tilde{W} \to l\bar{\tilde{\nu}}, \quad \bar{\tilde{\nu}} \to \bar{\nu}\tilde{\gamma} ; \tag{1.5a}$$

$$\tilde{Z} \to \nu\bar{\tilde{\nu}}, \quad \bar{\tilde{\nu}} \to \bar{\nu}\tilde{\gamma} \tag{1.5b}$$

are then dominant. Since in this case the $\tilde{Z}$ decays mainly into an unobservable mode we only consider the multilepton signals from $Z \to \tilde{W}\bar{\tilde{W}}$, which can be substantial. This signal would also be accessible at electron-positron colliders, particularly at the Stanford Linear Collider (SLC) and CERN LEP.

This paper is organized as follows. An $SU(3) \times SU(2) \times U(1)$-invariant supergravity model is presented in Sec. II. The chargino (λ_- and charged Higgs fermion) mass matrix is diagonalized exactly and the neutralino (λ_3, λ_1, and two neutral Higgs fermions) mass matrix is diagonalized approximately by assuming $m_{\tilde{\gamma}} \ll M_W$. All the interaction Lagrangians used in the paper are presented in terms of the mass eigenstates. In Sec. III we present all the lowest-order tree-level amplitudes which contribute to gaugino pair production allowing for off W and Z resonance production. All the helicity amplitudes are presented using the formalism of Ref. 26. Using this formalism, we can present the expressions for the amplitudes which are needed to calculate distributions of gaugino decay products with full spin correlations in a compact form which can be easily evaluated numerically. The amplitudes for $\tilde{W}$ and $\tilde{Z}$ decays are given in Sec. IV. The convolution of the production and decay amplitudes necessary for the calculation of the final particle (quark, lepton, and photino) distributions is also explained here. The reader who is interested only in the results but not in the technical details may skip Secs. III and IV without much loss of continuity. Numerical results on jet(s) + $\not{p}_T$ signals from the hadronic decays of $\tilde{W}$ and $\tilde{Z}$ may be found in Sec. V for both CERN and Tevatron collider energies.

The corresponding results for multilepton $+ \not{p}_T$ signals from the leptonic decays of $\widetilde{W}$ and $\widetilde{Z}$ are given in Sec. VI and for jet(s) plus lepton(s) $+ \not{p}_T$ events in Sec. VII. The single-lepton signature resulting from a $\widetilde{W}$ of mass greater than ≈ 45 GeV (produced mainly via $W \to \widetilde{W}\widetilde{\gamma}$) is examined in Sec. VIII. The case $v \neq v'$ is considered in Sec. IX, with the discussion mainly focusing on the possibility of a light scalar neutrino. Section X contains a summary of our results and our conclusions. The helicity-amplitude techniques[26] used in our computation are reviewed in Appendix A. Final expressions in a form particularly convenient for numerical evaluation of the complete spin-correlated amplitudes are listed in Appendix B.

II. THE SUPERSYMMETRIC MODEL

In this section we discuss the details of our model for the couplings and masses of supersymmetric particles. We envisage working with a minimal effective low-energy theory derived by integrating out the heavy degrees of freedom that are present in the fundamental theory. For obvious reasons, we will confine our attention to the gauge and Higgs sectors of the theory.

The couplings of the gauge and Higgs fermions to the electroweak gauge bosons are completely determined by $SU(2)_L \times U(1)_Y$ and supersymmetry. However, the gauge and Higgs fermions of the same charge mix to form the mass eigenstates once $SU(2)_L \times U(1)_Y$ is broken. These mixing angles, and hence the couplings of the mass eigenstates, are model dependent, but it is possible to parametrize all minimal SUSY models in terms of a few parameters.[19] It is this feature that makes any global discussion of gaugino production possible without considering each model on an individual basis.

In addition to the $SU(2)_L \times U(1)_Y$ gauge fermions, all SUSY models contain at least two Higgs doublets as it is not possible to give masses to both $T_{3_L} = +\frac{1}{2}$ and $T_{3_L} = -\frac{1}{2}$ quarks with just one Higgs field.[3] Also, because global SUSY models with supersymmetry being broken at a scale of ~ 1 TeV seem to have phenomenological difficulties,[27] we work within the framework of the $N=1$ supergravity models.[19] In these models, supersymmetry is broken in the *hidden sector* at a scale of $\sim 10^{11}$ GeV. The breaking of supersymmetry, which is felt by quarks, leptons, and gauge and Higgs bosons only via their gravitational interactions with the hidden sector, also induces vacuum expectation values for the Higgs field causing a breakdown of $SU(2)_L \times U(1)_Y$. Furthermore, in these models,[18] soft-SUSY-breaking mass terms are induced by the super Higgs mechanism.

The mass terms for the $SU(2)_L \times U(1)_Y$ gauge fermions λ and λ_0 and the Higgs fermions h and h', whose scalar partners give masses to the $T_{3_L} = +\frac{1}{2}$ and $T_{3_L} = -\frac{1}{2}$ quarks, respectively, take the form

$$(\bar{\lambda}_-, \bar{\chi}_-)(M_{(\text{charge})} P_L + M^T_{(\text{charge})} P_R) \begin{pmatrix} \lambda_- \\ \chi_- \end{pmatrix} \tag{2.1a}$$

for the charged sector, and

$$\tfrac{1}{2}(\bar{h}^0 \bar{h}^{0\prime} \bar{\lambda}_3 \bar{\lambda}_0)(M_{(\text{neutral})} P_L + M_{(\text{neutral})} P_R) \begin{pmatrix} h^0 \\ h^{0\prime} \\ \lambda_3 \\ \lambda_0 \end{pmatrix} \tag{2.1b}$$

for the neutral sector. In Eq. (2.1a), the Dirac spinors λ_-, χ_- are defined by

$$\lambda_- \equiv \frac{1}{\sqrt{2}}(\lambda_1 + i\lambda_2), \quad \chi_- \equiv P_L h' - P_R h$$

with h (h') and h^0 ($h^{0\prime}$) being shorthand notation for the charged and neutral components of the doublets h (h'), respectively. P_L (P_R) denotes the left (right) chirality projector. The mass matrices that appear in Eq. (2.1) are given by

$$M_{(\text{charge})} = \begin{pmatrix} \mu_2 & gv' \\ gv & 2m_1 \end{pmatrix}, \tag{2.2a}$$

$$M_{(\text{neutral})} = \begin{pmatrix} 0 & -2m_1 & +\frac{1}{\sqrt{2}}gv & -\frac{1}{\sqrt{2}}g'v \\ -2m_1 & 0 & -\frac{1}{\sqrt{2}}gv' & +\frac{1}{\sqrt{2}}g'v' \\ +\frac{1}{\sqrt{2}}gv & -\frac{1}{\sqrt{2}}gv' & +\mu_2 & 0 \\ -\frac{1}{\sqrt{2}}g'v & +\frac{1}{\sqrt{2}}g'v' & 0 & +\mu_1 \end{pmatrix}. \tag{2.2b}$$

In Eq. (2), $2m_1$ is the supersymmetric Higgs-fermion mixing mass term, μ_2 and μ_1 are soft-SUSY-breaking $SU(2)_L$ and $U(1)_Y$ gaugino masses, and v and v' are the vacuum expectation values of the Higgs scalars h and h'. In a grand unified theory with a common gaugino mass at the unification scale, μ_1 and μ_2 satisfy the relation[18,19]

$$\frac{\mu_1}{\mu_2} = \tfrac{5}{3}\tan^2\theta_W . \tag{2.3}$$

The analysis of these mass matrices has been carried out by a number of authors.[28] Here, we briefly review the SUSY-fermion mixings in order to elucidate our assumptions and also to set up the notation used in the rest of this paper.

We first concentrate on the diagonalization of the charged sector (2.1a). The mass matrix is diagonalized by rotating the left- and right-handed components of the fields by different angles γ_L and γ_R ($0\le\gamma_L,\ \gamma_R\le 180°$) given by[28]

$$\tan\gamma_L=(x_-)^{-1}\,, \tag{2.4a}$$

$$\tan\gamma_R=(y_-)^{-1}\,, \tag{2.4b}$$

with

$$x_-=\frac{(4m_1{}^2-\mu_2{}^2-2M_W{}^2\cos2\alpha)-\zeta}{2\sqrt{2}M_W(\mu_2\sin\alpha+2m_1\cos\alpha)}\,, \tag{2.5a}$$

$$y_-=\frac{(4m_1{}^2-\mu_2{}^2+2M_W{}^2\cos2\alpha)-\zeta}{2\sqrt{2}M_W(\mu_2\cos\alpha+2m_1\sin\alpha)}\,. \tag{2.5b}$$

Here

$$\tan\alpha=v'/v \tag{2.5c}$$

and

$$\zeta^2=(4m_1{}^2-\mu_2{}^2)^2+4M_W{}^2\times(M_W{}^2\cos^2 2\alpha+4m_1{}^2+\mu_2{}^2+4m_1\mu_2\sin2\alpha)\,. \tag{2.5d}$$

The eigenvalues are given by

$$m_\pm{}^2=\tfrac{1}{2}(4m_1{}^2+2M_W{}^2+\mu_2{}^2\pm\zeta)\,. \tag{2.6}$$

In the class of supergravity models[18] in which $SU(2)_L\times U(1)_Y$ breaking is radiatively driven by the Yukawa coupling of a top quark with mass ~40–50 GeV (Ref. 29), or in the simplest tree-breaking models[30] where $SU(2)_L\times U(1)_Y$ is broken at the tree level (Ref. 31) $v'/v\simeq1$. In this case, the mass matrix (2.1a) is particularly simple to diagonalize and we find the eigenstates $\tilde{W}_{(+)}$ and $\tilde{W}_{(-)}$ with eigenvalues m_+ and m_-, respectively, given by

$$\begin{bmatrix}\tilde{W}_{(+)}\\ \gamma_5\tilde{W}_{(-)}\end{bmatrix}=\begin{bmatrix}f_- & f_+\\ f_+ & -f_-\end{bmatrix}\begin{bmatrix}\lambda_-\\ \chi_-\end{bmatrix}$$

with

$$f_-\equiv\left[\frac{\mu_2+m_-}{m_++m_-}\right]^{1/2},\quad f_+\equiv\left[\frac{m_+-\mu_2}{m_++m_-}\right]^{1/2}. \tag{2.7a}$$

For $v'=v$, we have $\gamma_L=\gamma_R=\gamma$ with $f_+=\sin\gamma$ and $f_-=-\cos\gamma$. The masses $m_\pm$ then reduce to

$$m_\pm=\left|\left[\left[m_1-\frac{\mu_2}{2}\right]^2+M_W{}^2\right]^{1/2}\pm\left[m_1+\frac{\mu_2}{2}\right]\right|\,. \tag{2.7b}$$

The diagonalization of the neutralino sector is more cumbersome. In this paper we are interested in the production of light-gaugino states primarily via decays of gauge bosons. The neutralino states of interest are, therefore, those eigenstates ($\tilde{\gamma},\tilde{Z}$) that contain substantial fractions of the superpartners of the photon and Z^0 boson. Because the Higgs sector is very model dependent, we have not considered the decays of W,Z into Higgs fermions. We have assumed that the photino mass (and hence the SUSY-breaking gaugino mass) is small and so the decay $W\to\tilde{W}\tilde{\gamma}$ is almost always accessible as discussed earlier.[20] For $v'=v$, the second lightest neutralino state tends to have a large SU(2)-gaugino component and hence its coupling to the W boson is enhanced because it is a (weak) isovector. For v'/v rather different from unity, m_1 small and $\mu_2\simeq0$, this state becomes relatively heavy[33] and its production in association with $\tilde{W}_{(-)}$ from the decay of W is kinematically forbidden. If m_1 and μ_2 are substantially larger, then $W\to\tilde{W}\tilde{Z}$ can occur but then if v'/v is substantially less than one, the $\tilde{Z}$ decays via the invisible $\nu\bar{\nu}$ mode making the signal difficult to detect. If $v'/v\gg1$, then $\tilde{e}$ becomes the lightest scalar fermion. The ASP limit on the scalar-electron mass requires $m_{\tilde{e}}\gtrsim m_{\tilde{W}},m_{\tilde{Z}}$ and hence the decay patterns of the gauginos are similar to the $v'/v=1$ case. We have, therefore, diagonalized the neutralino sector only for the case $v'/v=1$.

Following Ref. 28, we proceed by first diagonalizing the neutralino system for $\mu_1=\mu_2=0$ and then incorporating these masses as perturbations on the zero-photino-mass eigenstates.

For $\mu_1=\mu_2=0$, the superpartner of the photon, $\tilde{\gamma}^{(0)}$ given by

$$-i\gamma_5\tilde{\gamma}^{(0)}\equiv\cos\theta_W\lambda_0+\sin\theta_W\lambda_3 \tag{2.8}$$

and is a zero-mass eigenstate. The other eigenstates are

$$-i\gamma_5\tilde{Z}^{(0)}_{(-)}\equiv\left[\frac{\mu_-}{2(\mu_++\mu_-)}\right]^{1/2}\left[-h^0+h'^0+\frac{\sqrt{2}M_Z}{\mu_-}(\cos\theta_W\lambda_3-\sin\theta_W\lambda_0)\right], \tag{2.9a}$$

$$\tilde{Z}^{(0)}_{(+)}\equiv\left[\frac{\mu_+}{2(\mu_++\mu_-)}\right]^{1/2}\left[h^0-h'^0+\frac{\sqrt{2}M_Z}{\mu_+}(\cos\theta_W\lambda_3-\sin\theta_W\lambda_0)\right], \tag{2.9b}$$

and

$$-i\gamma_5\tilde{h}^{(0)}\equiv\frac{1}{\sqrt{2}}(h^0+h'^0)\,, \tag{2.9c}$$

with the eigenvalues for the $\tilde{Z}^{(0)}_{(-)}$, $\tilde{Z}^{(0)}_{(+)}$, and $\tilde{h}^{(0)}$ being μ_-, μ_+, and $2m_1$, respectively.

In this analysis, we have tacitly assumed that $m_1>0$. The reason for the γ_5 transformation on the $\tilde{Z}^{(0)}_{(-)}$ and $\tilde{h}^{(0)}$ [the superscript (0) is to denote that these are eigenstates only if $m_{\tilde{\gamma}(0)}=0$] is that these eigenvectors have negative eigenvalue for the mass matrix (2.2b) with $v=v'$—the γ_5 flips the sign of the mass term and the factor i ensures that the fields are self-conjugate. For the zero-mass $\tilde{\gamma}^{(0)}$ state, that is purely a convention.

The eigenvalues $\mu_\pm$ satisfy[30]

$$\mu_+\mu_- \equiv M_Z{}^2 \ . \tag{2.10a}$$

Further, these are not independent of the eigenvalues for the charginos or $\tilde{h}^{(0)}$. We have

$$m_\pm = |[(m_1-\mu_2/2)^2+M_W{}^2]^{1/2} \pm (m_1+\mu_2/2)| \ , \tag{2.10b}$$

$$\mu_- = (m_1{}^2+M_Z{}^2)^{1/2}-m_1 \ . \tag{2.10c}$$

Thus if μ_2 (and hence $m_{\tilde{\gamma}}$) is zero, we may take the $\tilde{W}_{(-)}$ mass m_- to be a free parameter in terms of which all the masses are determined. We note that Eq. (2.10) implies that if $\mu_2=0$, there is a charged state $\tilde{W}_{(-)}$ and a neutral state $\tilde{Z}^{(0)}_{(-)}$ each of which is lighter than the W and Z^0, respectively. This is a consequence of the general result mentioned in the Introduction.

At this point it is worth pointing out the corresponding situation for tree-breaking models.[30] In this case, there is an extra singlet field U which modifies the neutralino mass matrix in Eq. (2.2b). Its couplings are such that the eigenstates $\tilde{\gamma}^{(0)}$ and $\tilde{Z}^{(0)}_{(\pm)}$ are left unchanged but the state $\tilde{h}^{(0)}$ picks up an extra component proportional to U. In addition, there is another eigenstate $\tilde{h}'^{(0)}$ which again depends on h^0, h'^0, and U alone. In this case, one of the masses (of $\tilde{h}^{(0)}$ or $\tilde{h}'^{(0)}$) may be chosen as an additional free parameter. For our purposes, it is sufficient to note that in both the radiative and tree-breaking models, the gauginos enter only in the $\tilde{\gamma}^{(0)}$ and $\tilde{Z}^{(0)}_{(\pm)}$ eigenstates. We will come back to this point shortly.

We now consider the effect of turning on the supersymmetry-breaking gaugino masses μ_1 and μ_2. Because these affect only the sector in which the gauginos enter, the states $\tilde{\gamma}^{(0)}$, $\tilde{Z}^{(0)}_{(-)}$, and $\tilde{Z}^{(0)}_{(+)}$ mix further, and their eigenvalues also shift from 0, μ_-, and μ_+. It is straightforward to work out the mass eigenstates[28] and the corresponding eigenvalues treating the gaugino masses in lowest-order perturbation theory. We find that the eigenstates $\tilde{\gamma}$, $\tilde{Z}_{(-)}$, and $\tilde{Z}_{(+)}$ are related to the states $\tilde{\gamma}^{(0)}$, $\tilde{Z}^{(0)}_{(-)}$, and $\tilde{Z}^{(0)}_{(+)}$ by

$$\begin{bmatrix} \tilde{Z}^{(0)}_{(-)} \\ \tilde{Z}^{(0)}_{(+)} \\ \tilde{\gamma}^{(0)} \end{bmatrix} = \begin{bmatrix} 1 & \delta & \epsilon_1 \\ -\delta & 1 & \epsilon_2 \\ -\epsilon_1 & -\epsilon_2 & 1 \end{bmatrix} \begin{bmatrix} \tilde{Z}_{(-)} \\ \tilde{Z}_{(+)} \\ \tilde{\gamma} \end{bmatrix} , \tag{2.11}$$

where

$$\epsilon_1 = \sqrt{2} N_1 \frac{M_Z}{\mu_-{}^2} \sin\theta_W \cos\theta_W (\mu_2-\mu_1) \ , \tag{2.12a}$$

$$\epsilon_2 = -\sqrt{2} N_2 \frac{M_Z}{\mu_+{}^2} \sin\theta_W \cos\theta_W (\mu_2-\mu_1) \ , \tag{2.12b}$$

and

$$\delta = \frac{2N_1N_2}{\mu_++\mu_-}(\mu_2\cos^2\theta_W+\mu_1\sin^2\theta_W) \ , \tag{2.12c}$$

with

$$N_{1,2} \equiv \left[\frac{\mu_{-,}\mu_+}{2(\mu_++\mu_-)} \right]^{1/2} .$$

The corresponding eigenvalues are

$$m_{\tilde{Z}_{(-)}} = \mu_- + \frac{\mu_+}{\mu_++\mu_-} |\mu_2\cos^2\theta_W+\mu_1\sin^2\theta_W| \ , \tag{2.13a}$$

$$m_{\tilde{Z}_{(+)}} = \mu_+ - \frac{\mu_-}{\mu_++\mu_-} |\mu_2\cos^2\theta_W+\mu_1\sin^2\theta_W| \ , \tag{2.13b}$$

and

$$m_{\tilde{\gamma}} = |\mu_2\sin^2\theta_W+\mu_1\cos^2\theta_W| \ . \tag{2.13c}$$

Here, θ_W denotes the electroweak mixing angle. We note that because we have chosen to define the photino with the γ_5 transformation [see Eq. (2.8)], we choose μ_1 and μ_2 as negative numbers.

In this paper, we will refer to the state $\tilde{Z}_{(-)}$ as the Z gaugino (and denote it by $\tilde{Z}$), the state $\tilde{Z}_{(+)}$ as the heavy Z gaugino ($\tilde{Z}_h$), and the state $\tilde{\gamma}$ as the photino. This is to be contrasted with the states $\tilde{h}$ and $\tilde{h}'$ which contain only the Higgs fermions. Similarly, we refer to the states $\tilde{W}_{(-)}$ and $\tilde{W}_{(+)}$ as the W gaugino ($\tilde{W}$) and heavy W gaugino ($\tilde{W}_h$), respectively. We emphasize here again that Eqs. (2.4)—(2.11) completely determine the mixing angles and hence the couplings to gauge bosons and matter fermions (and their scalar partners) in both radiative and tree-breaking models. Further, because the $\tilde{W}$'s and $\tilde{Z}$'s contain substantial weak isovector (gaugino) components, we may expect them to be copiously produced in $W^\pm$ and Z^0 decays.[22] This is to be contrasted with the Higgs-fermion states that have weaker isodoublet couplings to the gauge bosons. Their masses and couplings are more model dependent as has already been explained. For these reasons, we will not consider the Higgs-fermion state in the following.

The couplings of the $\tilde{W}$'s, $\tilde{Z}$'s, and photinos to the gauge bosons and to the matter can now be readily worked out from $SU(2)_L \times U(1)_Y$, supersymmetry, and the mixings. We find

$$\mathcal{L} = \mathcal{L}_{\text{standard}} + \mathcal{L}_{\text{gaugino}} + \mathcal{L}_{\text{gaugino—scalar-fermion}} \tag{2.14}$$

with

$$\mathcal{L}_{\text{standard}} = -ee_q\bar{q}\gamma^\mu q A_\mu - e\bar{q}\gamma^\mu(\alpha_q+\beta_q\gamma_5)qZ_\mu - \frac{g}{\sqrt{2}}\left[\bar{u}\gamma^\mu\left[\frac{1-\gamma_5}{2}\right]dW^+_\mu + \bar{\nu}\gamma^\mu\left[\frac{1-\gamma_5}{2}\right]eW^+_\mu + \text{H.c.}\right] , \tag{2.15a}$$

where

$$
\begin{aligned}
&e_u=\tfrac{2}{3},\quad e_d=-\tfrac{1}{3}\,,\\
&\alpha_u=-(\tfrac{1}{4}\cot\theta_W-\tfrac{5}{12}\tan\theta_W)\,,\\
&\alpha_d=-(\tfrac{1}{12}\tan\theta_W-\tfrac{1}{4}\cot\theta_W)\,,\\
&\beta_u=\tfrac{1}{4}(\cot\theta_W+\tan\theta_W)\,,\\
&\beta_d=-\tfrac{1}{4}(\cot\theta_W+\tan\theta_W)\,.
\end{aligned}
\tag{2.15b}
$$

The gaugino Lagrangian reads

$$
\begin{aligned}
\mathcal{L}_{\text{gaugino}}=&\,e\bar{\tilde W}\gamma^\mu\tilde W A_\mu-e\cot\theta_W\bar{\tilde W}\gamma^\mu(x_c-y_c\gamma_5)\tilde W Z_\mu\\
&+[\bar{\tilde W}\gamma^\mu(iA+B\gamma_5)\tilde\gamma W_\mu\\
&+\bar{\tilde W}\gamma^\mu(iC+D\gamma_5)\tilde Z W_\mu+\text{H.c.}]\,,
\end{aligned}
\tag{2.16a}
$$

where

$$
\begin{aligned}
x_c&=1-\tfrac{1}{4}\sec^2\theta_W(\cos^2\gamma_L+\cos^2\gamma_R)\,,\\
y_c&=\tfrac{1}{4}\sec^2\theta_W(\cos^2\gamma_R-\cos^2\gamma_L)\,,\\
A&=g\sin\theta_W\left[\frac{\sin^2\gamma_L+\sin^2\gamma_R}{2}\right]\\
&\quad+\left[\frac{g}{\sqrt{2}}N_1 f_- +g\sqrt{2}N_1\frac{f_+M_Z}{\mu_-}\cos\theta_W\right]\epsilon_1\,,\\
B&=+ig\sin\theta_W\left[\frac{\sin^2\gamma_R-\sin^2\gamma_L}{2}\right]\\
&\quad+\left[\frac{gf_-}{\sqrt{2}}N_2-gf_+\sqrt{2}\frac{M_Z}{\mu_+}\cos\theta_W\right]\epsilon_2\,;
\end{aligned}
\tag{2.16b}
$$

$$
\begin{aligned}
C&=\left[\frac{g}{\sqrt{2}}N_1 f_- +g\sqrt{2}N_1 f_+\frac{M_Z}{\mu_-}\cos\theta_W\right]\\
&\quad-gf_+\sin\theta_W\epsilon_1\,,\\
D&=\left[\frac{gf_-}{\sqrt{2}}N_2-\frac{\sqrt{2}gf_+N_2M_Z}{\mu_+}\cos\theta_W\right]\delta\,.
\end{aligned}
\tag{2.16c}
$$

The terms proportional to ϵ_1, ϵ_2, and δ in (2.16b) and (2.16c) are corrections due to mixings induced by $\mu_2\neq0$. The couplings x_c,y_c and the leading terms in the couplings A and B have been computed for arbitrary values of v'/v while the $W\tilde W\tilde Z$ couplings C and D in (2.16c) and the corrections terms in (2.16b) have been computed only for $v'/v=1$. In this case, the $W\tilde W\tilde\gamma$ couplings A and B reduce to

$$
\begin{aligned}
A&=gf_+\sin\theta_W\\
&\quad+\left[\frac{g}{\sqrt{2}}N_1 f_- +g\sqrt{2}N_1 f_+\frac{M_Z}{\mu_-}\cos\theta_W\right]\epsilon_1\,,\\
B&=\left[\frac{gf_-}{\sqrt{2}}N_2-gf_+\sqrt{2}N_2\frac{M_Z}{\mu_+}\cos\theta_W\right]\epsilon_2\,.
\end{aligned}
\tag{2.16d}
$$

Notice that the $Z\tilde W\bar{\tilde W}$ and the dominant piece in the $W\tilde W\tilde\gamma$ coupling become vector when $v'/v=1$. The SUSY-breaking gaugino masses also induce axial-vector pieces which are numerically small unless the $\tilde Z$ mass is close to M_Z. Finally,

$$
\begin{aligned}
\mathcal{L}_{\text{gaugino-scalar-fermion}}=&\,e\tilde f_L^\dagger\bar{\tilde\gamma}(iX_f+Y_f)\frac{1-\gamma_5}{2}f+e\tilde f_R^\dagger\bar{\tilde\gamma}(iX'_f+Y'_f)\frac{1+\gamma_5}{2}f+\text{H.c.}\\
&+e\tilde f_L^\dagger\bar{\tilde Z}(iP_f+Q_f)\frac{1-\gamma_5}{2}f+e\tilde f_R^\dagger\bar{\tilde Z}(iP'_f+Q'_f)\frac{1+\gamma_5}{2}f+\text{H.c.}\\
&-g\sin\gamma_L\tilde d_L^\dagger\overline{\tilde W^c}\frac{1-\gamma_5}{2}u+g\sin\gamma_R\tilde u_L^\dagger\bar{\tilde W}\frac{1-\gamma_5}{2}d\\
&-g\sin\gamma_L\tilde l_L^\dagger\overline{\tilde W^c}\frac{1-\gamma_5}{2}\nu+g\sin\gamma_R\tilde\nu^\dagger\bar{\tilde W}\frac{1-\gamma_5}{2}l+\text{H.c.}
\end{aligned}
\tag{2.17}
$$

with $f=l,\nu,u,d$. The values of the parameters X, Y, X', Y', P, Q, P', and Q' are listed in Table I.

The masses of the W gaugino, photino, and Z gaugino (along with those of the heavy W and Z gauginos) are determined in terms of the parameters μ_2 and μ_1. Alternatively, we may choose $m_{\tilde\gamma}$ instead of μ_2 [see Eqs. (2.3) and (2.13c)] and $m_{\tilde W}\equiv m_-$ [see Eq. (2.10b)] as arbitrary parameters in terms of which the remaining masses and all the couplings are determined. The only remaining arbitrariness is the masses of the scalar partners of the fermions. Assuming a common scalar mass m_0, at the unification scale, the radiatively corrected masses at a scale of ~100 GeV have been worked out. We have, for three effective generations in the β function (and $\sin^2\theta_W=0.22$) (Refs. 25 and 34),

TABLE I. The parameters that enter into Eq. (2.17). Here, $t \equiv \tan\theta_W$ and $c \equiv \cot\theta_W$.

f	l	ν	u	d
X_f	$-\sqrt{2}+\frac{N_1M_Z}{\mu_-}(t-c)\epsilon_1$	$\frac{N_1M_Z}{\mu_-}\frac{1}{\sin\theta_W\cos\theta_W}\epsilon_1$	$\frac{2\sqrt{2}}{3}+\frac{N_1M_Z}{\mu_-}(c-\frac{1}{3}t)\epsilon_1$	$\frac{-\sqrt{2}}{3}-\frac{N_1M_Z}{\mu_-}(c+\frac{1}{3}t)\epsilon_1$
Y_f	$\frac{-N_2M_Z}{\mu_+}(t-c)\epsilon_2$	$\frac{-N_2M_Z}{\mu_+}\frac{1}{\sin\theta_W\cos\theta_W}\epsilon_2$	$\frac{-N_2M_Z}{\mu_+}(c-\frac{1}{3}t)\epsilon_2$	$\frac{N_2M_Z}{\mu_+}(c+\frac{1}{3}t)\epsilon_2$
X_f'	$-\sqrt{2}+\frac{2N_1M_Z}{\mu_-}t\epsilon_1$	0	$\frac{2\sqrt{2}}{3}-\frac{4}{3}\frac{N_1M_Z}{\mu_-}t\epsilon_1$	$\frac{-\sqrt{2}}{3}+\frac{2}{3}\frac{N_1M_Z}{\mu_-}t\epsilon_1$
Y_f'	$\frac{2N_2M_Z}{\mu_+}t\epsilon_2$	0	$\frac{-4}{3}\frac{N_2M_Z}{\mu_+}t\epsilon_2$	$\frac{2}{3}\frac{N_2M_Z}{\mu_+}\epsilon_2$
P_f	$\frac{N_1M_Z}{\mu_-}(t-c)+\sqrt{2}\epsilon_1$	$\frac{N_1M_Z}{\mu_-}\frac{1}{\sin\theta_W\cos\theta_W}$	$\frac{N_1M_Z}{\mu_-}(c-\frac{1}{3}t)-\frac{2}{3}\sqrt{2}\epsilon_1$	$\frac{-N_1M_Z}{\mu_-}(c+\frac{1}{3}t)+\frac{\sqrt{2}}{3}\epsilon_1$
Q_f	$\frac{N_2M_Z}{\mu_+}(t-c)\delta$	$\frac{N_2M_Z}{\mu_+}\frac{1}{\sin\theta_W\cos\theta_W}\delta$	$\frac{N_2M_Z}{\mu_+}(c-\frac{1}{3}t)\delta$	$\frac{-N_2M_Z}{\mu_+}(c+\frac{1}{3}t)\delta$
P_f'	$\frac{2N_1M_Z}{\mu_-}t+\sqrt{2}\epsilon_1$	0	$-\frac{4}{3}\frac{N_1M_Z}{\mu_-}t-\frac{2\sqrt{2}}{3}\epsilon_1$	$\frac{2}{3}\frac{N_1M_Z}{\mu_-}t+\frac{\sqrt{2}}{3}\epsilon_1$
Q_f'	$\frac{-2N_2M_Z}{\mu_+}t\delta$	0	$\frac{4}{3}\frac{N_2M_Z}{\mu_+}t\delta$	$\frac{-2}{3}\frac{N_2M_Z}{\mu_+}t\delta$

$$\begin{aligned}
m^2(\tilde{d}_L)&=m_0{}^2+0.43rM_Z{}^2+30.2m_{\tilde{\gamma}}{}^2\ ,\\
m^2(\tilde{d}_R)&=m_0{}^2+0.07rM_Z{}^2+28.4m_{\tilde{\gamma}}{}^2\ ,\\
m^2(\tilde{u}_L)&=m_0{}^2-0.36rM_Z{}^2+30.2m_{\tilde{\gamma}}{}^2\ ,\\
m^2(\tilde{u}_R)&=m_0{}^2-0.14rM_Z{}^2+28.4m_{\tilde{\gamma}}{}^2\ ,\\
m^2(\tilde{e}_L)&=m_0{}^2+0.28rM_Z{}^2+2.2m_{\tilde{\gamma}}{}^2\ ,\\
m^2(\tilde{e}_R)&=m_0{}^2+0.22rM_Z{}^2+0.6m_{\tilde{\gamma}}{}^2\ ,\\
m^2(\tilde{\nu})&=m_0{}^2-0.50rM_Z{}^2+2.2m_{\tilde{\gamma}}{}^2\ ,
\end{aligned} \tag{2.18a}$$

where

$$r=\frac{v^2-v'^2}{v^2+v'^2}\ . \tag{2.18b}$$

In Eq. (2.18a), the second term comes from the D terms which make contributions of the form $M_Z{}^2(-T_{3_f}+e_f\sin^2\theta_W)r$ for superpartners of left-handed fermions and with the opposite sign for those of right-handed fermions. The last term comes from the evolution of the common scalar mass from the unification scale down to a scale of $\sim M_W$. As expected, these corrections are bigger for the strongly interacting quark sector than for the weakly interacting lepton sector.

We note that for $r>0$ it is possible for the scalar neutrinos to be very light. Such a scalar neutrino, even if produced, may have escaped detection.[35,36] In this paper, we will first concentrate on the $v'/v=1$ case ($r=0$), but will return to examine some consequences of light scalar neutrinos ($v'/v\neq1$) in Sec. IX.

For $v'/v=1$, we see that the mass splitting between the $T_{3_L}=+\frac{1}{2}$ and $T_{3_L}=-\frac{1}{2}$ scalar fermions is small provided $m_{\tilde{\gamma}}$ is not too large. We have restricted our analysis to $m_{\tilde{\gamma}}\lesssim 10$ GeV (recall that we have diagonalized the neutralino sector under the assumption that $|\mu_1|$, $|\mu_2| \ll M_W, 2m_1$). We are focusing on scalar-quark masses exceeding ~ 100 GeV. In this case, the scalar leptons are roughly degenerate with the scalar quarks, an assumption we have made in the computation of the $\tilde{W}$ and $\tilde{Z}$ branching ratio.

III. THE PRODUCTION OF GAUGINOS

In this section we present all the amplitudes that contribute to gaugino pair ($\tilde{W}\tilde{\gamma}, \tilde{W}\tilde{Z}, \tilde{W}^+\tilde{W}^-$) production at hadron colliders in lowest order. The $\tilde{W}$- and $\tilde{Z}$-decay amplitudes will be given in the next section. It is almost hopeless to evaluate the squared matrix elements for the full process incorporating correctly the spin correlations among decay particles using usual trace techniques. Although, in principle, the calculation can be done with the help of algebraic manipulation programs, the result of such a calculation would be extraordinarily long and cause numerical inefficiency. For example, even assuming the W pole dominance for $q\bar{q}\to\tilde{W}\tilde{Z}$, there are 12 amplitudes for each hadronic final state, and hence, 78 terms each involving four often lengthy traces need to be evaluated. The calculation is made manageable by the direct computation of the helicity amplitudes. We find the formalism of Ref. 26 well suited for this purpose. In order to render this paper self-contained, we briefly review in Appendix A the basic ingredients of the helicity-basis calculus which is necessary to reproduce all our results. Further details may be found in Ref. 26.

Shown in Fig. 1 are the lowest-order Feynman diagrams that contribute to gaugino pair production at hadron colliders. Figures 1(a)–1(c) contribute to the parton subprocess

$$d(q,\sigma)+\bar{u}(\bar{q},\bar{\sigma})\to\tilde{W}^-(p_1,s_1)+\tilde{\gamma}(p_2,s_2) \tag{3.1a}$$

or

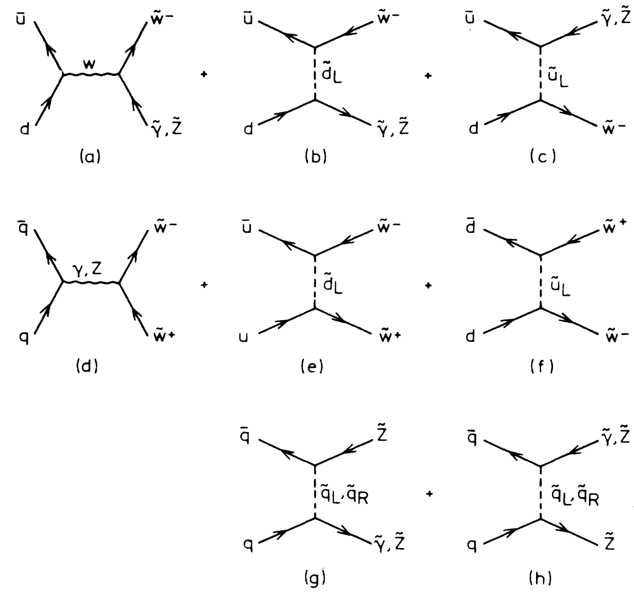

FIG. 1. The lowest-order Feynman diagrams which contribute to the processes (a)—(c) $d\bar u \to \tilde W^- \tilde\gamma$ or $d\bar u \to \tilde W^- \tilde Z$, (d)—(f) $q\bar q \to \tilde W^- \tilde W^+$, and (g) and (h) $q\bar q \to \tilde Z\tilde\gamma$ or $\tilde Z\tilde Z$. Solid, dashed, and wavy lines denote fermions, scalars, and vectors, respectively. Arrows denote fermion number flow.

$$d(q,\sigma)+\bar u(\bar q,\bar\sigma)\to \tilde W^-(p_1,s_1)+\tilde Z(p_2,s_2)\ , \tag{3.1b}$$

while Figs. 1(d)—1(f) contribute to the subprocess

$$q(q,\sigma)+\bar q(\bar q,\bar\sigma)\to \tilde W^-(p_1,s_1)+\tilde W^+(p_2,s_2)\ . \tag{3.1c}$$

Here the four-momenta and helicity of each particle is shown in parentheses. These three are the only uncolored-gaugino-pair-production processes which have a chance to have s-channel W- or Z-resonance contribution at hadron colliders. The processes

$$q(q,\sigma)+\bar q(\bar q,\bar\sigma)\to \tilde Z(p_1,s_1)+\tilde\gamma(p_2,s_2) \tag{3.1d}$$

and

$$q(q,\sigma)+\bar q(\bar q,\bar\sigma)\to \tilde Z(p_1,s_1)+\tilde Z(p_2,s_2) \tag{3.1e}$$

have no s-channel resonance contribution as shown by Figs. 1(g) and 1(h), and hence their cross sections remain small at CERN/Tevatron collider energies even for light $\tilde Z$. [The supersymmetric partner of the photon ($\tilde\gamma^{(0)}$) does not couple to the Z^0 since the gauge boson is electrically neutral. Thus, the coupling of the $\tilde\gamma$ to Z^0 can arise only from the mixing induced via $m_{\tilde\gamma}\neq 0$, which as discussed in Sec. III, we have taken to be small. For $v=v'$, the $Z^0\tilde Z\tilde Z$ coupling also vanishes whereas as discussed in Sec. IX the $\tilde Z$ tends to be heavy when $v\neq v'$.] We remind the reader that $\tilde W$, $\tilde Z$, and $\tilde\gamma$ denote the mass eigenstates of the charged or neutral gauge-Higgs-fermion sector and in general they are a mixture of pure gaugino and Higgs-fermion states. The mixing angles, and hence all their couplings, have been determined based on the supergravity model discussed in Sec. II.

The helicity amplitudes for each subprocess are expressed as sums of contributing diagrams:

$$\mathcal{M}(d\bar u\to \tilde W^-\tilde V;\sigma,\bar\sigma,s_1,s_2)=\mathcal{M}_{\rm a}^{(\tilde V)}+\mathcal{M}_{\rm b}^{(\tilde V)}+\mathcal{M}_{\rm c}^{(\tilde V)}\ , \tag{3.2a}$$

for $\tilde V=\tilde\gamma$ or $\tilde Z$, and

$$\mathcal{M}(u\bar u\to \tilde W^-\tilde W^+;\sigma,\bar\sigma,s_1,s_2)=\mathcal{M}_{\rm d}^{(u)}+\mathcal{M}_{\rm e}\ , \tag{3.2b}$$

$$\mathcal{M}(d\bar d\to \tilde W^-\tilde W^+;\sigma,\bar\sigma,s_1,s_2)=\mathcal{M}_{\rm d}^{(d)}+\mathcal{M}_{\rm f}\ , \tag{3.2c}$$

$$\mathcal{M}(q\bar q\to \tilde Z\tilde V;\sigma,\bar\sigma,s_1,s_2)=\mathcal{M}_{\rm g}^{(\tilde V)}+\mathcal{M}_{\rm h}^{(\tilde V)}\ . \tag{3.2d}$$

It is straightforward to evaluate all eight contributing diagrams from the interaction Lagrangians listed in the preceding section. We first present all the amplitudes in the usual four-spinor basis:

$$\mathcal{M}_{\rm a}^{(\tilde V)}=g_-^{udW}\sum_{\lambda=\pm} g_\lambda^{\tilde W\tilde V W}D_W^{\mu\nu}(q+\bar q)\bar v(\bar q,\bar\sigma)\gamma_\mu P_- u(q,\sigma)\bar u(p_1,s_1)\gamma_\nu P_\lambda v(p_2,s_2)\ , \tag{3.3a}$$

$$\mathcal{M}_{\rm b}^{(\tilde V)}=g_-^{u\tilde W\tilde d}g_-^{\tilde V d\tilde d}D_{\tilde d_-}(q-p_2)\bar v(\bar q,\bar\sigma)P_+ v(p_1,s_1)\bar u(p_2,s_2)P_- u(q,\sigma)\ , \tag{3.3b}$$

$$\mathcal{M}_{\rm c}^{(\tilde V)}=-g_-^{\tilde W d\tilde u}g_-^{u\tilde V\tilde u}D_{\tilde u_-}(q-p_1)\bar v(\bar q,\bar\sigma)P_+ v(p_2,s_2)\bar u(p_1,s_1)P_- u(q,\sigma)\ , \tag{3.3c}$$

$$\mathcal{M}_{\rm d}^{(q)}=\sum_{V=\gamma,Z}\sum_{\lambda=\pm}\sum_{\tau=\pm} g_\lambda^{qqV}g_\tau^{\tilde W\tilde W V}D_V^{\mu\nu}(q+\bar q)\bar v(\bar q,\bar\sigma)\gamma_\mu P_\lambda u(q,\sigma)\bar u(p_1,s_1)\gamma_\nu P_\tau v(p_2,s_2)\ , \tag{3.3d}$$

$$\mathcal{M}_{\rm e}=g_-^{u\tilde W\tilde d}g_-^{\tilde W u\tilde d}D_{\tilde d_-}(q-p_2)\bar v(\bar q,\bar\sigma)P_+ v(p_1,s_1)\bar u(p_2,s_2)P_- u(q,\sigma)\ , \tag{3.3e}$$

$$\mathcal{M}_{\rm f}=-g_-^{d\tilde W\tilde u}g_-^{\tilde W d\tilde u}D_{\tilde u_-}(q-p_1)\bar v(\bar q,\bar\sigma)P_+ v(p_2,s_2)\bar u(p_1,s_1)P_- u(q,\sigma)\ , \tag{3.3f}$$

$$\mathcal{M}_{g}^{(\tilde V)}=\sum_{\lambda=\pm} g_\lambda^{q\tilde Z\tilde q}g_\lambda^{\tilde V q\tilde q}D_{\tilde q_\lambda}(q-p_2)\bar v(\bar q,\bar\sigma)P_{-\lambda} v(p_1,s_1)\bar u(p_2,s_2)P_\lambda u(q,\sigma)\ , \tag{3.3g}$$

$$\mathcal{M}_{\rm h}^{(\tilde V)}=-\sum_{\lambda=\pm} g_\lambda^{q\tilde V\tilde q}g_\lambda^{\tilde Z q\tilde q}D_{\tilde q_\lambda}(q-p_1)\bar v(\bar q,\bar\sigma)P_{-\lambda} v(p_2,s_2)\bar u(p_1,s_1)P_\lambda u(q,\sigma)\ . \tag{3.3h}$$

Here, $P_\pm=(1\pm\gamma_5)/2$ are the chiral projectors and we denote $\tilde{q}_L$ by $\tilde{q}_-$ and $\tilde{q}_R$ by $\tilde{q}_+$ for notational convenience. The scalar propagator factor is defined as

$$D_\phi(k)=[k^2-m_\phi{}^2+i\theta(k^2)m_\phi\Gamma_\phi]^{-1} \tag{3.4}$$

and the covariant vector-boson propagator factor is expressed in terms of the above as

$$D_V^{\mu\nu}(k)=D_V(k)\begin{cases}-g^{\mu\nu}+k^\mu k^\nu/m_V{}^2 & \text{if } m_V\neq 0\ ,\\ -g^{\mu\nu} & \text{if } m_V=0\ .\end{cases} \tag{3.5}$$

The relative sign of the amplitudes and the convention for choosing u or v spinors are determined by directly applying the Wick expansion and by employing the explicit plane-wave expressions

$$\psi(x)=\int\frac{d^3k}{(2\pi)^2 2k_0}\sum_{s=\pm}[b_s(k)u(k,s)e^{-ik\cdot x} + d_s^\dagger(k)v(k,s)e^{ik\cdot x}]\ , \tag{3.6a}$$

$$\psi^c(x)=\eta_c\int\frac{d^3k}{(2\pi)^3 2k_0}\sum_{s=\pm}[d_s(k)u(k,s)e^{-ik\cdot x} + b_s^\dagger(k)v(k,s)e^{ik\cdot x}]\ , \tag{3.6b}$$

and with $\eta_c=1$ by convention. Here ψ^c, the charge-conjugate spinor, satisfies

$$\psi_c(x)=\eta_c C\bar{\psi}(x)^T\ , \tag{3.7}$$

where use has been made of the relation (A9). Majorana fields ($\tilde{\gamma}$ and $\tilde{Z}$) are self-conjugate:

$$\psi(x)=\psi^c(x)=C\bar{\psi}^T(x)\ . \tag{3.8}$$

With these conventions, the amplitudes (3.3) involve neither the charge-conjugation matrix C nor Majorana phase factors explicitly.

All the couplings are determined by the Lagrangian presented in Sec. II:

$$g_-^{udW}=(g_-^{duW})^*=g/\sqrt{2}\ , \tag{3.9a}$$

$$g_\pm^{qq\gamma}=ee_q,\quad g_\pm^{qqZ}=e(\alpha_q\pm\beta_q)\ , \tag{3.9b}$$

$$g_\pm^{\tilde{W}\tilde{W}\gamma}=-e,\quad g_\pm^{\tilde{W}\tilde{W}Z}=e\cot\theta_W(x_c\mp y_c)\ , \tag{3.9c}$$

$$g_\pm^{\tilde{W}\tilde{\gamma}W}=(g_\pm^{\tilde{\gamma}\tilde{W}W})^*=-(iA\pm B)\ ,\quad g_\pm^{\tilde{W}\tilde{Z}W}=(g_\pm^{\tilde{Z}\tilde{W}W})^*=-(iC\pm D)\ , \tag{3.9d}$$

$$g_-^{\tilde{W}d\tilde{u}}=(g_-^{d\tilde{W}\tilde{u}})^*=-g\sin\gamma_R\ ,\quad g_-^{\tilde{W}u\tilde{d}}=(g_-^{u\tilde{W}\tilde{d}})^*=+g\sin\gamma_L\ , \tag{3.9e}$$

$$g_-^{\tilde{\gamma}q\tilde{q}}=(g_-^{q\tilde{\gamma}\tilde{q}})^*=-e(iX_q+Y_q)\ ,\quad g_+^{\tilde{\gamma}q\tilde{q}}=(g_+^{q\tilde{\gamma}\tilde{q}})^*=-e(iX'_q+Y'_q)\ , \tag{3.9f}$$

$$g_-^{\tilde{Z}q\tilde{q}}=(g_-^{q\tilde{Z}\tilde{q}})^*=-e(iP_q+Q_q)\ ,\quad g_+^{\tilde{Z}q\tilde{q}}=(g_+^{q\tilde{Z}\tilde{q}})^*=-e(iP'_q+Q'_q)\ . \tag{3.9g}$$

The various constants that appear above have been listed in Eqs. (2.15) and (2.16), and Table I. Here we remark that our helicity amplitudes are expressed in terms of very general couplings and hence can be readily used for even more general cases simply by replacing the couplings listed in Eq. (3.9).

Following the method[26] outlined in Appendix A, it is straightforward to express all the amplitudes (3.3) in terms of the quantities $\omega_\lambda(k)$ and $T(p,k)_{\lambda_T}$ which can easily be evaluated numerically [see Eqs. (A3), (A4), and (A11) for their definitions]. The complete results are listed in Appendix B in a form which allows direct numerical evaluation.

We now present the total production rates for various gaugino-pair-production processes at both CERN ($\sqrt{s}=630$ GeV) and Fermilab Tevatron ($\sqrt{s}=2$ TeV) energies. The total cross section summed over final polarization and averaged over initial polarization for a generic subprocess

$$q(q,\sigma)+\bar{q}'(\bar{q},\bar{\sigma})\rightarrow\tilde{V}_1(p_1,s_1)+\tilde{V}_2(p_2,s_2) \tag{3.10}$$

reads

$$\hat{\sigma}(q\bar{q}'\rightarrow\tilde{V}_1\tilde{V}_2) =\int\frac{1}{2\hat{s}}\frac{1}{4}\sum_\sigma\sum_{\bar{\sigma}}\sum_{s_1}\sum_{s_2}|\mathcal{M}(\sigma,\bar{\sigma},s_1,s_2)|^2 S\frac{d\hat{t}}{8\pi\hat{s}}\ , \tag{3.11}$$

where the statistical factor $S=1$ ($\frac{1}{2}$) when $\tilde{V}_1\neq\tilde{V}_2$ ($\tilde{V}_1=\tilde{V}_2$) and

$$\hat{s}=(q+\bar{q})^2,\quad \hat{t}=(q-p_1)^2\ . \tag{3.12}$$

A convolution with effective parton distribution gives the total cross section in $p\bar{p}$ collisions as

$$\sigma(p\bar{p}\rightarrow\tilde{V}_1\tilde{V}_2X)=\sum_{a,b}\int dx\int d\bar{x}\, D_{a/p}(x,\hat{s})D_{b/\bar{p}}(\bar{x},\hat{s})\hat{\sigma}(ab\rightarrow\tilde{V}_1\tilde{V}_2)\delta\left[\frac{\hat{s}}{s}-x\bar{x}\right]\ . \tag{3.13}$$

We use the set-1 parton distributions of Duke and Owens with $\Lambda=0.2$ GeV (Ref. 37) throughout the paper. Other numerical parameters are fixed as $\alpha=e^2/4\pi=\frac{1}{128}$, $\sin^2\theta_W=0.22$, $M_W=83$ GeV, $M_Z=94$ GeV, $\Gamma_W^0=2.82$ GeV, and $\Gamma_Z^0=2.83$ GeV, where the superscripts 0 denote the width without the supersymmetry contribution we are considering. The total widths which enter in the propagators (3.5) should read

$$\Gamma_V=\Gamma_V^0+\Delta\Gamma_V\quad \text{for } V=W \text{ or } Z\ , \tag{3.14}$$

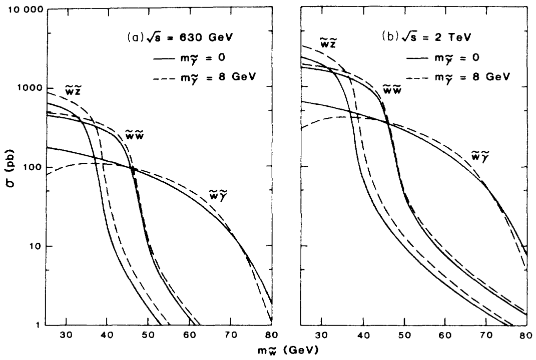

FIG. 2. Total cross sections for production of $\tilde{W}\tilde{Z}$, $\tilde{W}\tilde{W}$, and $\tilde{W}\tilde{\gamma}$ pairs as a function of $m_{\tilde{W}}$ by $p\bar{p}$ collisions for $m_{\tilde{\gamma}}=0$ (solid lines) and $m_{\tilde{\gamma}}=8$ GeV (dashed lines) at (a) $\sqrt{s}=630$ GeV and (b) $\sqrt{s}=2$ TeV. In this figure, $v'/v=1$ and $m_{\tilde{q}}=200$ GeV. The $\tilde{Z}$ mass is determined in terms of $m_{\tilde{W}}$ and $m_{\tilde{\gamma}}$ and is typically a few GeV greater than $m_{\tilde{W}}$.

where $\Delta\Gamma_V$ denote the gaugino-pair-production contributions and are given in Ref. 38.

Shown in Fig. 2 are the total cross sections for gaugino pair production expected in the supergravity model with $m_{\tilde{\gamma}}=0$ or 8 GeV and $v'=v$. Substantial cross sections are expected only when resonance decays $W\to\tilde{V}_1\tilde{V}_2$ or $Z\to\tilde{V}_1\tilde{V}_2$ are kinematically allowed. The cross sections are indeed sensitive to variations in the photino mass, not only near the kinematic cutoff for gauge-boson decay, but also for small values of $m_{\tilde{W}}$ as is illustrated by the $\tilde{W}\tilde{\gamma}$ curve—here, mixing effects decrease the $W\tilde{W}\tilde{\gamma}$ coupling constant causing as much as a factor of 2 decrease in cross section.

In Fig. 3 (Fig. 4) we illustrate for completeness the cross sections for $\tilde{Z}\tilde{\gamma}$ ($\tilde{Z}\tilde{Z}$) production. These cross sections, at both $\sqrt{s}=630$ and 2000 GeV, are generally less than 1 pb for $m_{\tilde{q}}>100$ GeV, so these reactions are likely to be inconsequential in the search for supersymmetry at $p\bar{p}$ colliders.

Large contributions to the W and Z widths due to decays to gauginos can affect the hadron-collider estimates for the number of neutrinos. When low statistics do not

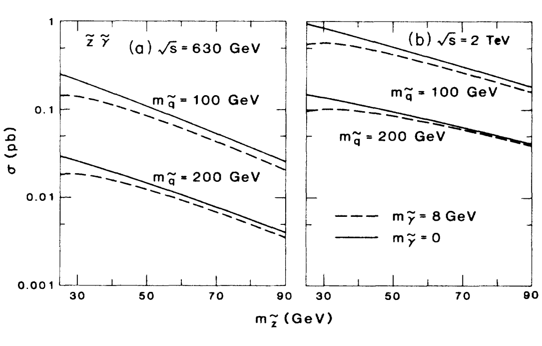

FIG. 3. Total cross section for $p\bar{p}\to\tilde{Z}\tilde{\gamma}X$ for $m_{\tilde{q}}=100$ or 200 GeV and $m_{\tilde{\gamma}}=0$ (solid lines) and $m_{\tilde{\gamma}}=8$ GeV (dashed lines) at (a) $\sqrt{s}=630$ GeV and (b) $\sqrt{s}=2$ TeV for $v'/v=1$.

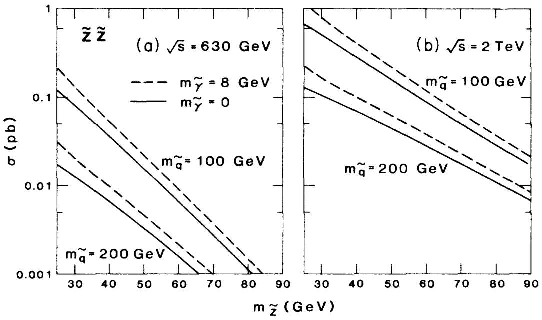

FIG. 4. Total cross section for $p\bar{p}\to\tilde{Z}\tilde{Z}X$ for $m_{\tilde{q}}=100$ or 200 GeV and $m_{\tilde{\gamma}}=0$ (solid lines) and $m_{\tilde{\gamma}}=8$ GeV (dashed lines) at (a) $\sqrt{s}=630$ GeV and (b) $\sqrt{s}=2$ TeV and for $v'/v=1$.

allow for an accurate measurement of the total Z width, it is convenient[39] to confront the experimentally observed ratio

$$R=\sigma(p\bar{p}\to ZX;Z\to e\bar{e})/\sigma(p\bar{p}\to WX;W\to e\bar{\nu})\ , \qquad (3.15)$$

with theoretical expectations.[40,23] In Fig. 5, we present[41] the ratio R as a function of $m_{\tilde{W}}$ for $m_{\tilde{\gamma}}=0$ (solid line) and 8 GeV (dashed line) for $v'/v=1$, and for $m_{\tilde{\gamma}}=0$ for $v'/v=0.5$ (dotted-dashed line). The results presented are for $\sqrt{s}=630$ GeV; they scarcely change for $\sqrt{s}=2$ TeV. Also shown is the standard-model (SM) prediction for three light neutrino species; the UA1 experimental measurement[42] of R is shown as a band. We see the entire range of $m_{\tilde{W}}$ is consistent with experiment; furthermore, for the $v'/v=1$ case there are two values of $m_{\tilde{W}}$ which exactly agree with the SM (one value of $m_{\tilde{W}}$ for $v'/v=0.5$). At best, the R parameter may eventually restrict same values of $m_{\tilde{W}}$ but can never rule out certain values of low-mass gauginos. We now turn to a discussion of the decays of $\tilde{W}$ and $\tilde{Z}$.

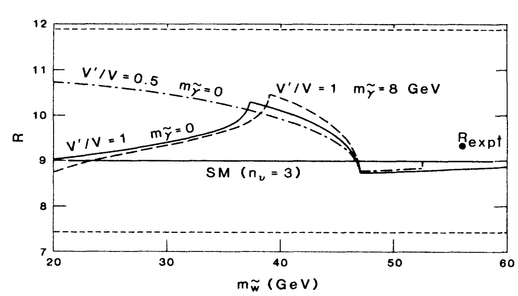

FIG. 5. Gaugino-pair contribution to the ratio R of $Z\to e^+e^-$ and $W\to e\bar{\nu}$ events observed in $p\bar{p}$ collisions at $\sqrt{s}=630$ GeV. The standard-model contribution for three light neutrinos is denoted as SM, and the measured value from UA1 Collaboration is shown as the solid circle marked $R_{\rm expt}$ with horizontal dashed lines on either side indicating the quoted experimental errors. We illustrate R for supergravity models when $v'/v=1$ for $m_{\tilde{\gamma}}=0$ (solid line) and 8 GeV (dashed line) and for $v'/v=0.5$ and $m_{\tilde{\gamma}}=0$ (dotted-dashed line).

IV. THE DECAYS OF GAUGINOS

In this section, we present all the lowest-order amplitudes for $\widetilde{W}$ and $\widetilde{Z}$ decays within the framework of the general supergravity model discussed in Sec. II. We also show at the end of this section how to combine the production amplitudes of Sec. III and these decay amplitudes in order to produce exclusive parton-level decay distributions with complete spin correlations.

When scalar fermions (scalar quarks and leptons) are heavier than the $\widetilde{W}$, which is the case we are studying, it decays into a photino and a light-fermion pair:

$$\widetilde{W}^-(p,s)\to\widetilde{\gamma}(k_1,\lambda_1)+f(k_2,\lambda_2)+\bar{F}(k_3,\lambda_3)\ , \tag{4.1a}$$

$$\widetilde{W}^+(p,s)\to\widetilde{\gamma}(k_1,\lambda_1)+\bar{f}(k_2,\lambda_2)+F(k_3,\lambda_3)\ , \tag{4.1b}$$

where a pair (f,F) can either be (d,u), (s,c), (b,t), or (l,ν_l) with $l=e,\mu,\tau$. In most cases the decay mode $\widetilde{W}^-\to\widetilde{\gamma}b\bar{t}$ is severely suppressed by phase space or even forbidden. In our analysis, we neglect this decay mode entirely. The Feynman diagrams contributing to the $\widetilde{W}^-$ decay (4.1a) are shown in Figs. 6(i)–6(k).

The $\widetilde{Z}$ has three decay modes:

$$\widetilde{Z}(p,s)\to\widetilde{\gamma}(k_1,\lambda_1)+f(k_2,\lambda_2)+\bar{f}(k_3,\lambda_3) \tag{4.2a}$$

$$\to\widetilde{W}^-(k_1,\lambda_1)+F(k_2,\lambda_2)+\bar{f}(k_3,\lambda_3) \tag{4.2b}$$

$$\to\widetilde{W}^+(k_1,\lambda_1)+\bar{F}(k_2,\lambda_2)+f(k_3,\lambda_3)\ . \tag{4.2c}$$

The decay (4.2a) always occurs since the photino is assumed to be light and the latter two occur in our supergravity model with $m_{\widetilde{\gamma}}\ll M_W$ and $v=v'$ (see Sec. II) since the $\widetilde{W}$ is always lighter than the $\widetilde{Z}$. Figures 6(l) and 6(m) contribute to the decay $\widetilde{Z}\to\widetilde{\gamma}f\bar{f}$ (4.2a) and three diagrams, Figs. 6(n)–6(p) contribute to the decay $\widetilde{Z}\to\widetilde{W}^-F\bar{f}$ (4.2b). The decay $\widetilde{Z}\to\widetilde{\gamma}f\bar{f}$ is allowed for five light-quark and three charged-lepton flavors whereas the decay $\widetilde{Z}\to\widetilde{W}^-f\bar{F}$ occurs for two light families of quarks $(f,F)=(d,u)$, (s,c), and three families of leptons (l,ν).

The helicity amplitude for each decay process can be expressed as a sum of contributions from each diagram. Suppressing four-momenta labels of each particle, we can write the $\widetilde{W}$-decay amplitudes as

$$\mathscr{M}(\widetilde{W}^-\to\widetilde{\gamma}f\bar{F};s,\lambda_1,\lambda_2,\lambda_3)\equiv\mathscr{M}_i+\mathscr{M}_j+\mathscr{M}_k\ . \tag{4.3a}$$

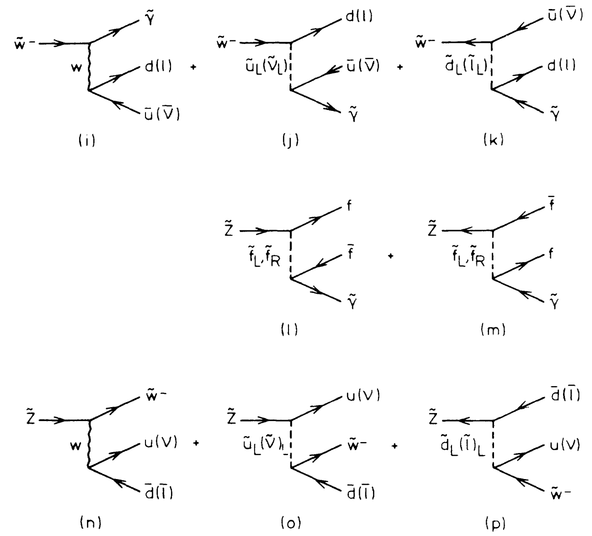

FIG. 6. Lowest-order Feynman diagrams which contribute to the decay of (i)–(k) $\widetilde{W}^-$ and (l)–(p) $\widetilde{Z}$.

We note that the amplitudes for $\widetilde{W}^+$ decays are related to those for $\widetilde{W}^-$ decays because CP is conserved at the tree level. We have

$$\mathscr{M}(\widetilde{W}^+\to\widetilde{\gamma}\bar{f}F;s,\lambda_1,\lambda_2,\lambda_3)=s\lambda_1\lambda_2\lambda_3\mathscr{M}(\widetilde{W}^-\to\widetilde{\gamma}f\bar{F};-s,-\lambda_1,-\lambda_2-\lambda_3)^*\ . \tag{4.3b}$$

The $\widetilde{Z}$ decay amplitudes are similarly written as

$$\mathscr{M}(\widetilde{Z}\to\widetilde{\gamma}f\bar{f};s,\lambda_1,\lambda_2,\lambda_3)=\mathscr{M}_{\rm l}+\mathscr{M}_{\rm m}\ , \tag{4.3c}$$

$$\mathscr{M}(\widetilde{Z}\to\widetilde{W}^-F\bar{f};s,\lambda_1,\lambda_2,\lambda_3)=\mathscr{M}_{\rm n}+\mathscr{M}_{\rm o}+\mathscr{M}_{\rm p}\ , \tag{4.3d}$$

with the amplitude for $\widetilde{Z}\to\widetilde{W}^+\bar{F}f$ again being related to (4.3d) by CP invariance. Hence, we only need to evaluate the eight diagrams shown in Fig. 6.

We present all the amplitudes in the usual four-spinor notation below:

$$\mathscr{M}_{\rm i}=\sum_\lambda g_\lambda^{\widetilde{\gamma}\widetilde{W}W}g_-^{du\,W}D_W^{\mu\nu}(k_2+k_3)\bar{u}(k_1,\lambda_1)\gamma_\mu P_\lambda u(p,s)\bar{u}(k_2,\lambda_2)\gamma_\nu P_- v(k_3,\lambda_3)\ , \tag{4.4a}$$

$$\mathscr{M}_{\rm j}=-g_-^{d\widetilde{W}\tilde{u}}g_-^{\widetilde{\gamma}u\tilde{u}}D_{\tilde{u}_-}(k_1+k_3)\bar{u}(k_2,\lambda_2)P_+u(p,s)\bar{u}(k_1,\lambda_1)P_-v(k_3,\lambda_3)\ , \tag{4.4b}$$

$$\mathscr{M}_{\rm k}=g_-^{\widetilde{W}u\tilde{d}}g_-^{d\widetilde{\gamma}\tilde{d}}D_{\tilde{d}_-}(k_1+k_2)\bar{v}(p,s)P_-v(k_3,\lambda_3)\bar{u}(k_2,\lambda_2)P_+v(k_1,\lambda_1)\ , \tag{4.4c}$$

$$\mathscr{M}_{\rm l}=-\sum_\lambda g_\lambda^{f\widetilde{Z}\tilde{f}}g_\lambda^{\gamma f\tilde{f}}D_{\tilde{f}_\lambda}(k_1+k_3)\bar{u}(k_2,\lambda_2)P_{-\lambda}u(p,s)\bar{u}(k_1,\lambda_1)P_\lambda v(k_3,\lambda_3)\ , \tag{4.4d}$$

$$\mathscr{M}_{\rm m}=\sum_\lambda g_\lambda^{\widetilde{Z}f\tilde{f}}g_\lambda^{f\widetilde{\gamma}\tilde{f}}D_{\tilde{f}_\lambda}(k_1+k_2)\bar{v}(p,s)P_\lambda v(k_3,\lambda_3)\bar{u}(k_2,\lambda_2)P_{-\lambda}v(k_1,\lambda_1)\ , \tag{4.4e}$$

$$\mathscr{M}_{\rm n}=\sum_\lambda g_\lambda^{\widetilde{W}\widetilde{Z}W}g_-^{u\,dW}D_W^{\mu\nu}(k_2+k_3)\bar{u}(k_1,\lambda_1)\gamma_\mu P_\lambda u(p,s)\bar{u}(k_2,\lambda_2)\gamma_\nu P_-v(k_3,\lambda_3)\ , \tag{4.4f}$$

$$\mathcal{M}_{\rm o}=-g_{-}^{u\tilde{Z}\tilde{u}}g_{-}^{\tilde{W}d\tilde{u}}D_{\tilde{u}_{-}}(k_1+k_3)\bar{u}(k_2,\lambda_2)P_{+}u(p,s)\bar{u}(k_1,\lambda_1)P_{-}v(k_3,\lambda_3)\ , \tag{4.4g}$$

$$\mathcal{M}_{\rm p}=g_{-}^{\tilde{Z}d\tilde{d}}g_{-}^{u\tilde{W}\tilde{d}}D_{\tilde{d}_{-}}(k_1+k_2)\bar{v}(p,s)P_{-}v(k_3,\lambda_3)\bar{u}(k_2,\lambda_2)P_{+}v(k_1,\lambda_1)\ . \tag{4.4h}$$

Here $\tilde{f}_{-}$ and $\tilde{f}_{+}$ stand for $\tilde{f}_L$ and $\tilde{f}_R$, respectively, and $\tilde{u}_{-}=\tilde{u}_L, \tilde{d}_{-}=\tilde{d}_L$. The expressions for each amplitude, in forms convenient for numerical evaluation, are listed in Appendix B. In these expressions, the quark and lepton masses are neglected for simplicity whereas gaugino masses are kept arbitrary. As emphasized in Ref. 26, there is no practical difficulty in also taking into account quark and lepton masses in the formalism whenever necessary. In all our applications, we neglect masses of the first five quark flavors and the six lepton flavors. We have also neglected any top-quark contributions. All the couplings that appear in Eq. (4.4) have been listed in Eq. (3.9). [The leptonic couplings are obtained from these simply by replacing the indices as $u\to\nu$, $d\to l$, and $q\to\nu$ or l in Eq. (3.9).]

It is worth mentioning at this point that all the decay amplitudes listed in Fig. 6 and in Eq. (4.4) are just obtained by crossing the production amplitudes listed in Fig. 1. One of the virtues of the formalism of Ref. 26 is that the crossing of helicity amplitudes is straightforward. There is no need to repeat the amplitude calculation again, apart from the trivial change in particle indices. All the decay amplitudes listed in Appendix B have been obtained from the corresponding production amplitudes by following the crossing prescription of Ref. 26.

Although our main purpose is to study distributions of gaugino decay products, partial widths and branching fractions are needed to normalize the cross section. Since $\tilde{W}$ decay occurs either via W or $\tilde{q}_L$ ($\tilde{l}_L$) exchange, the leptonic branching fraction could *a priori* depend on the scalar-fermion mass. It has been shown,[43] however, that for $m_{\tilde{\gamma}}=0$ unless $m_{\tilde{W}}$ is close to $m_{\tilde{q}}$ ($\approx m_{\tilde{l}}$), this branching fraction is essentially $\frac{1}{9}$, independent of scalar-fermion mass. Moreover, this is also a lower limit on the leptonic branching fraction. In our computation, we have evaluated this branching fraction exactly keeping $m_{\tilde{\gamma}}=8$ GeV. For $m_{\tilde{q}}\approx m_{\tilde{l}}\gtrsim 100$ GeV and $m_{\tilde{W}}\lesssim m_W$, we find an almost constant value of 11%, irrespective of $m_{\tilde{q}}$ ($\approx m_{\tilde{l}}$) and $m_{\tilde{\gamma}}$ for $m_{\tilde{\gamma}}\lesssim 10$ GeV.

The partial widths for the decays $\tilde{Z}\to f\bar{f}\tilde{\gamma}$ and $\tilde{Z}\to F\bar{f}\tilde{W}^{-}+\bar{F}f\tilde{W}^{+}$ can be readily calculated from the amplitudes via

$$\Gamma(\tilde{Z}\to\tilde{\gamma}f\bar{f})=\int\frac{1}{2m_{\tilde{Z}}}\sum_{\lambda_1}\sum_{\lambda_2}\sum_{\lambda_3}|\mathcal{M}(s,\lambda_1,\lambda_2,\lambda_3)|^2 d\Phi_3\ , \tag{4.5a}$$

$$\Gamma(\tilde{Z}\to\tilde{W}^{-}F\bar{f})=\int\frac{1}{2m_{\tilde{Z}}}\times\sum_{\lambda_1}\sum_{\lambda_2}\sum_{\lambda_3}|\mathcal{M}(s,\lambda_1,\lambda_2,\lambda_3)|^2 d\Phi_3\ , \tag{4.5b}$$

with the Lorentz-invariant phase-space factor

$$d\Phi_n\left[p=\sum_{i=1}^{n}k_i\right]=(2\pi)^4\delta^4\left[p-\sum_{i=1}^{n}k_i\right]\prod_{i=1}^{n}\frac{d^3k_i}{(2\pi)^3 2k_i^0}\ . \tag{4.6}$$

We have checked that the partial widths obtained are independent of the $\tilde{Z}$ momentum and helicity. As has been stressed in Ref. 26, Lorentz invariance provides us with a nontrivial check on the calculation.

The branching fractions for the two decay modes of the $\tilde{Z}$ are shown in Fig. 7. It is clear that unless $m_{\tilde{q}}$ ($\approx m_{\tilde{l}}$) exceeds ≈ 350 GeV the $\tilde{W}$ mode is suppressed relative to the $\tilde{\gamma}$ mode for $m_{\tilde{Z}}=45$ GeV. For smaller values of $m_{\tilde{Z}}$, an even higher scalar-fermion mass is needed for the two modes to have equal widths. We have, therefore, neglected the $Z\to\tilde{W}$ decay completely in this paper.

For the case when only the photino decay mode of the $\tilde{Z}$ is relevant, the leptonic branching fraction per lepton flavor takes a particularly simple form for degenerate scalar fermions. We have

$$\frac{\Gamma(\tilde{Z}\to l\bar{l}\tilde{\gamma})}{\Gamma(\tilde{Z}\to\text{everything})}=\frac{X_l{}^2P_l{}^2+X'_l{}^2P'_l{}^2}{n_l(X_l{}^2P_l{}^2+X'_l{}^2P'_l{}^2)+3n_u(X_u{}^2P_u{}^2+X'_u{}^2P'_u{}^2)+3n_d(X_d{}^2P_d{}^2+X'_d{}^2P'_d{}^2)}\ , \tag{4.7}$$

where we have neglected the numerically small constants Y_f and Q_f induced via the mixing of the heavy $\tilde{Z}$ (see Sec. II). In Eq. (4.7), n_l, n_u, and n_d are the number of lepton, up-quark, and down-quark families that are accessible via $\tilde{Z}$ decay. We note that (4.7) is independent of the scalar-fermion mass. Because of the mixings induced by $m_{\tilde{\gamma}}\neq 0$, the branching fraction depends on $m_{\tilde{Z}}$ and varies from 18% for $m_{\tilde{Z}}=26$ GeV to 14% for $m_{\tilde{Z}}=52$ GeV for $m_{\tilde{\gamma}}=8$ GeV. For $m_{\tilde{\gamma}}=0$, the branching fraction is 13% for all $\tilde{Z}$ masses.

We are now in a position to calculate the distributions of gaugino decay products at hadron colliders. Let us consider a generic gaugino-pair- ($\widetilde{V}_1\widetilde{V}_2$) production process followed by their decays:

$$\begin{aligned} q(q,\sigma)+\bar{q}'(\bar{q},\bar{\sigma}) &\to \widetilde{V}_1(p_1,s_1)+\widetilde{V}_2(p_2,s_2)\ , \\ \widetilde{V}_1(p_1,s_1) &\to \widetilde{\gamma}(k_1,\lambda_1)+f_2(k_2,\lambda_2)+\bar{f}_3(k_3,\lambda_3)\ , \\ \widetilde{V}_2(p_2,s_2) &\to \widetilde{\gamma}(k_4,\lambda_4)+f_5(k_5,\lambda_5)+\bar{f}_6(k_6,\lambda_6)\ . \end{aligned} \tag{4.8}$$

If $\widetilde{V}_2$ happens to be a $\widetilde{\gamma}$, then the last cascade process does not take place. On the other hand if $\widetilde{V}_2$ decays into $\widetilde{W}^-$, then the last line of Eq. (4.8) should be replaced, e.g., by an even longer cascade process (we have not considered this here),

$$\begin{aligned} \widetilde{V}_2(p_2,s_2) &\to \widetilde{W}^-(p_3,s_3)+f_5(k_5,\lambda_5)+\bar{f}_6(k_6,\lambda_6)\ , \\ \widetilde{W}^-(p_3,s_3) &\to \widetilde{\gamma}(k_4,\lambda_4)+f_7(k_7,\lambda_7)+\bar{f}_8(k_8,\lambda_8)\ . \end{aligned} \tag{4.9}$$

Of course, $\widetilde{V}_1$ can also have a similar decay chain. In the remainder of this paper, we consider only the $\widetilde{W}\widetilde{W}$, $\widetilde{W}\widetilde{\gamma}$, and $\widetilde{W}\widetilde{Z}$ production processes, the cross sections for which are enhanced by the resonance production of $W^{\pm}$ and Z^0. In our computation, however, we have retained the effect of all the Feynman graphs (see Fig. 1) that can contribute at the lowest order and have also retained finite-width effects.

We present as an example the cross section for the six-parton production process (4.8). By suppressing the particle and momentum indices whereas retaining only the helicity indices, the full production amplitude can be expressed as a product of the production amplitude and the two decay amplitudes, summed over intermediate gaugino helicities:

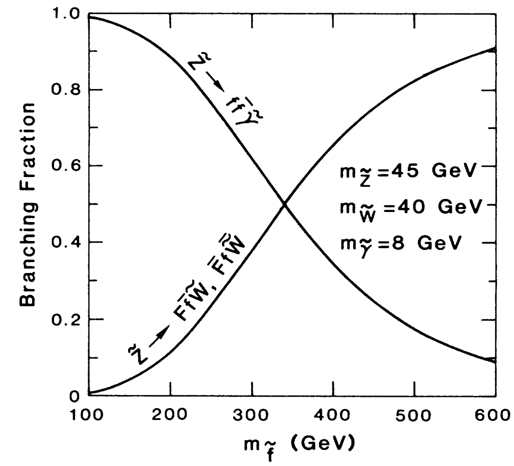

FIG. 7. The dependence of the branching fraction for $\widetilde{Z}\to f\bar{f}\widetilde{\gamma}$ and $\widetilde{Z}\to F\bar{f}\widetilde{W}+\bar{F}f\widetilde{W}$ on the scalar-fermion mass is shown for $m_{\widetilde{\gamma}}=8$ GeV assuming degenerate scalar fermions. We have illustrated the case for the maximal $\widetilde{Z}-\widetilde{W}$ mass difference for the range of $\widetilde{W}$ and $\widetilde{Z}$ masses relevant to our calculation so as to maximize the $\widetilde{W}$ decay mode, i.e., for smaller $\widetilde{Z}$ ($\widetilde{W}$) masses the cross over of the curves occurs for even higher scalar-fermion mass than in the figure.

$$\begin{aligned} \mathcal{M}(\sigma,\bar{\sigma};\lambda_i) &\equiv \mathcal{M}(\sigma,\bar{\sigma};\lambda_1,\lambda_2,\lambda_3,\lambda_4,\lambda_5,\lambda_6) \\ &= \sum_{s_1}\sum_{s_2}\mathcal{M}(\sigma,\bar{\sigma};s_1,s_2)\mathcal{M}(s_1;\lambda_1,\lambda_2,\lambda_3)\mathcal{M}(s_2;\lambda_4,\lambda_5,\lambda_6)D_{\widetilde{V}_1}(p_1)D_{\widetilde{V}_2}(p_2)\ . \end{aligned} \tag{4.10}$$

The quantum-mechanical superposition of different intermediate gaugino helicity states gives rise to the correlations among decaying particles. Strictly speaking, the expression (4.10) is valid only when the zero-width approximation holds for intermediate gauginos,

$$|D_{\widetilde{V}_1}(p_1)D_{\widetilde{V}_2}(p_2)|^2 \simeq \frac{\pi}{m_{\widetilde{V}_1}\Gamma_{\widetilde{V}_1}}\frac{\pi}{m_{\widetilde{V}_2}\Gamma_{\widetilde{v}_2}}\delta(p_1{}^2-m_{\widetilde{V}_1}{}^2)\delta(p_2{}^2-m_{\widetilde{V}_2}{}^2)\ , \tag{4.11}$$

which is indeed valid in all our applications. The polarization blind subprocess cross section is then obtained by

$$d\hat{\sigma}(q\bar{q}'\to\widetilde{\gamma}\,\widetilde{\gamma}f_2\bar{f}_3f_5\bar{f}_6)=\frac{1}{2\hat{s}}\frac{1}{4}\sum_{\sigma}\sum_{\bar{\sigma}}\left[\prod_{j=1}^{6}\sum_{\lambda_j}\right]|\mathcal{M}(\sigma,\bar{\sigma};\lambda_i)|^2 d\Phi_6 \tag{4.12}$$

with the invariant phase space (4.6). Since each helicity amplitude is just a complex number, Eq. (4.12) involves just a summation over absolute value squared of several different complex numbers which are indexed by the external particle helicities. The phase-space factor can be simplified by the zero-width approximation for intermediate gauginos. We get

$$\begin{aligned} |D_{\widetilde{V}_1}(p_1)D_{\widetilde{V}_2}(p_2)|^2 d\Phi_6\left[q+\bar{q}=\sum_{i=1}^{6}k_i\right] &= \left[\sum_{i=1}^{2}\frac{1}{2m_{\widetilde{V}_i}\Gamma_{\widetilde{V}_i}}\right]d\Phi_2(q+\bar{q}=p_1+p_2) \\ &\quad\times d\Phi_3(p_1=k_1+k_2+k_3)d\Phi_3(p_2=k_4+k_5+k_6)\ . \end{aligned} \tag{4.13}$$

Convolution with effective parton distributions finally give distributions in $p\bar{p}$ collisions as

$$d\sigma(p\bar{p}\to\widetilde{\gamma}\,\widetilde{\gamma}f_2\bar{f}_3f_5\bar{f}_6X)=\sum_{a,b}\int dx\int d\bar{x}\,D_{a/p}(x,\hat{s})D_{b/\bar{p}}(\bar{x},\hat{s})\delta\left[\frac{\hat{s}}{s}-x\bar{x}\right]d\hat{\sigma}(ab\to\widetilde{\gamma}\,\widetilde{\gamma}f_2\bar{f}_3f_5\bar{f}_6)\ . \tag{4.14}$$

A study of these distributions forms the subject of the rest of this paper.

V. JET SIGNALS FROM THE HADRONIC DECAYS OF THE GAUGINOS

In this section, we discuss the numerical results of our calculation of multijet + $\not{p}_T$ signals resulting from the hadronic decay of $\tilde{W}$ and $\tilde{Z}$ at CERN and at Fermilab Tevatron energies. In our computation, we have included the effects of $W^{\pm}$ and Z^0 being off mass shell and also the contributions to the production amplitudes from the t-channel exchange of the scalar quark. For definiteness, we have fixed the scalar-quark mass at 200 GeV. Our results are insensitive to any particular choice, reflecting the fact that the $W^{\pm}$ (Z^0) resonance dominates the production.

Throughout our computation we use the parton distributions of Ref. 37 (Set I), a QCD-motivated K factor of 1.4 and smearing due to the $W^{\pm}$ (Z^0) transverse motion according to the formula[44]

$$\frac{d\sigma}{dQ_T{}^2} \simeq e^{-25Q_T/\sqrt{s}} . \tag{5.1}$$

We have also attempted to include the acceptances and measurement resolutions of a realistic detector—the UA1 detector for $\sqrt{s}=630$ GeV and the Collider Detector at Fermilab Tevatron (CDF) for $\sqrt{s}=2$ TeV. Obviously, a treatment of these and also the trigger conditions depends on the detector, and hence is different for CERN and Fermilab energies. We have *not* treated the effects of hadronization, i.e., all our partons are identified with jets provided they pass the experimental cuts and triggers which we now discuss.

For CERN energies ($\sqrt{s}=630$ GeV) we have required that all jets are within the pseudorapidity acceptance:

$$|\eta_{\rm jet}| < 2.5 . \tag{5.2}$$

We have coalesced partons with $\Delta r \le 1$ where $\Delta r^2 = \Delta\eta^2 + \Delta\phi^2$, where $\Delta\phi$ is the azimuthal angle difference. We have assumed that a (multi)jet event can be triggered by any *one* of the following triggers:[45]

$$\text{(i)}\quad E_{T\rm jet} > 25 \text{ GeV} , \tag{5.3a}$$

$$\text{(ii)}\quad E_T^{\rm scalar} > 80 \text{ GeV} , \tag{5.3b}$$

or

$$|E_T(L) - E_T(R)| > 17 \text{ GeV and } E_{T\rm jet} > 15 \text{ GeV} . \tag{5.3c}$$

In Eq. (5.3b), $E_T^{\rm scalar}$ is the total scalar energy in the event and is given by

$$E_T^{\rm scalar} = \sum_{partons} E_T + E_T^s , \tag{5.4}$$

where E_T^s is the scalar energy in the residual event and is fluctuated according to[46]

$$\frac{dN}{dE_T^s} \simeq \frac{4E_T^s}{\langle E_T^s\rangle^2} \exp\left[-\frac{2E_T^s}{\langle E_T^s\rangle}\right] , \tag{5.5}$$

with $\langle E_T^s\rangle = 45$ GeV.

In addition to the triggers (5.3), we have the following selection criteria which must all be met before an event is considered acceptable.

(i) $\not{p}_T > \max(4\sigma, 15 \text{ GeV})$ where $\sigma = 0.7 \text{ GeV } (E_T^{\rm scalar}/\text{GeV})^{1/2}$.

(ii) $E_{T\rm jet} > 12$ GeV.

(iii) The $\not{p}_T$ vector should not point within 20° in azimuth of the vertical.

(iv) The $\not{p}_T$ vector should be isolated, i.e., there should be no hadronic activity with $E_T > 8$ GeV within 30° in azimuth of $\not{p}_T$.

(v) Finally, for an event to be labeled a monojet, we require that there is no hadronic activity exceeding 8 GeV back to back with the jet and within 30° in azimuth. In a real detector, there is a nonzero resolution on the measurement of hadronic p_T. In our computation, we have smeared the hadronic energy by a Gaussian of width

$$\Delta E = 0.8 \text{ GeV}(E/\text{GeV})^{1/2} . \tag{5.6}$$

We have attempted also to approximately model the acceptances and cuts for the CDF. In this, we have been guided by conversations with our experimental colleagues. For $\sqrt{s}=2$ TeV, we require

$$|\eta_{\rm jet}| < 4.0 , \tag{5.7a}$$

$$E_{T\text{fast jet}} > 25 \text{ GeV} , \tag{5.7b}$$

$$E_{T\rm jet} > 12 \text{ GeV}, \tag{5.7c}$$

and

$$\not{p}_T > 25 \text{ GeV} . \tag{5.7d}$$

Also, we coalesce jets within $\Delta r < 0.5$ rather than $\Delta r \le 1$ as for UA1. We have retained the isolation of the $\not{p}_T$ vector and the monojet selection criteria (iv) and (v) discussed above but have removed the $\pm 20°$ crack in the vertical direction. We have retained only the trigger (5.3a) [see (5.7b)] but have dropped triggers (ii) and (iii). Finally, we

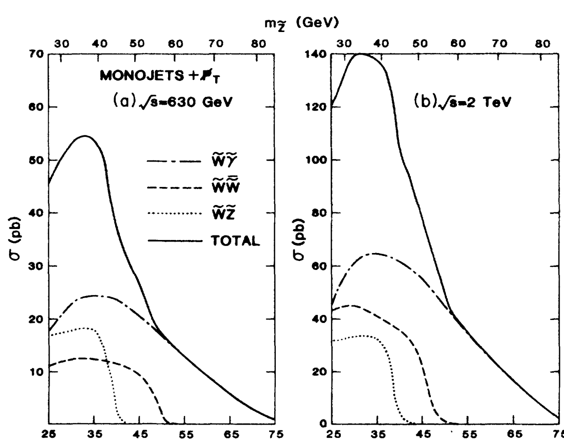

FIG. 8. Cross section for monojet-plus-$\not{p}_T$ signals expected when both $\tilde{W}$ and $\tilde{Z}$ decay hadronically, as a function of $m_{\tilde{W}}$ (lower scale) or $m_{\tilde{Z}}$ (upper scale) for $m_{\tilde{\gamma}}=8$ GeV and for (a) $\sqrt{s}=630$ GeV and (b) $\sqrt{s}=2$ TeV. The cuts are as described in Sec. V.

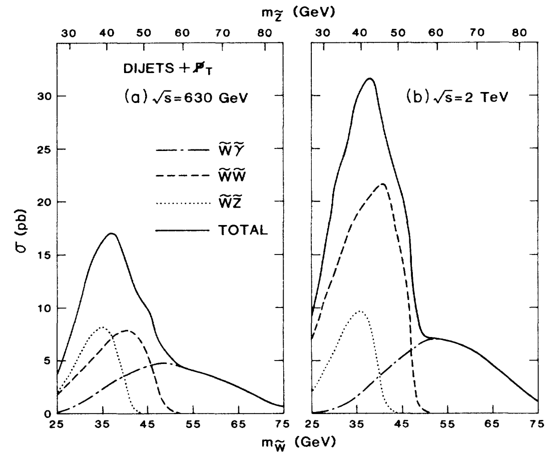

FIG. 9. Cross sections for dijet + $\not{p}_T$ signals as a function of the gaugino masses for (a) $\sqrt{s}=630$ GeV and (b) $\sqrt{s}=2$ TeV.

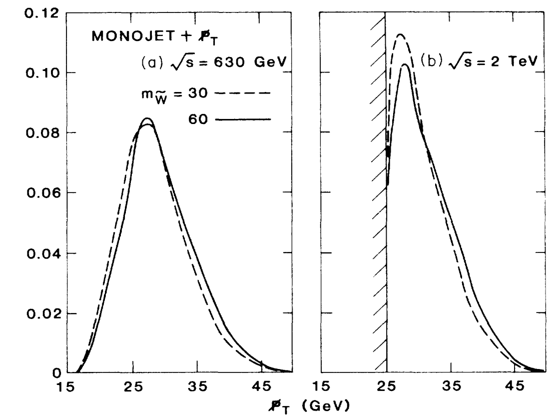

FIG. 10. Missing-p_T ($\not{p}_T$) distributions in monojet + $\not{p}_T$ events for $m_{\widetilde{W}}=30$ and 60 GeV. The cuts at (a) $\sqrt{s}=630$ GeV and (b) $\sqrt{s}=2$ TeV are as described in the text. $\widetilde{W}$ and $\widetilde{Z}$ decay hadronically and $m_{\widetilde{\gamma}}=8$ GeV.

have assumed the same energy resolution [Eq. (5.6)] as for UA1.

At this point, we note that not all the triggers [(5.3a)–(5.3c)] were active throughout the full UA1 run. Since it is not the purpose of this paper to analyze the data, we have not put in the three triggers weighted by the respective running times that they were operational. Rather, we study the various signals using conditions that we believe are realizable (or have been realized) at operational detectors, and try to indicate the mass limits that may be extractable from existing or soon to exist data. We now turn to a discussion of our results.

The monojet cross section as a function of the $\widetilde{W}$ mass (lower scale) or $\widetilde{Z}$ mass (upper scale) is shown for both CERN and Fermilab energies in Fig. 8. It is clear that monojets from $W\to\widetilde{W}\widetilde{\gamma}$ dominate in spite of a lower total cross section for $p\bar{p}\to\widetilde{W}\widetilde{\gamma}+X$. For low $\widetilde{W}$ masses, this is largely due to the fact that a much greater fraction of $\widetilde{W}\widetilde{\gamma}$ events pass the $\not{p}_T$ cut whereas for higher masses, $\widetilde{W}\widetilde{Z}$ and $\widetilde{W}\widetilde{W}$ production is kinematically suppressed. At the Tevatron we have higher cross sections but not as high as one might expect from a naive scaling of the $W^{\pm}$- and Z^0-production cross sections. This is, of course, due to the different cut and trigger conditions for the two cases. A curious feature at the Tevatron is the dominance of the $Z^0\to\widetilde{W}\overline{\widetilde{W}}$ over the $W\to\widetilde{W}\widetilde{Z}$ even for small $\widetilde{W}$ and $\widetilde{Z}$ masses.

This feature is even more pronounced for the dijet cross sections as may be seen from Fig. 9. For dijets, the $W\to\widetilde{W}\widetilde{Z}$ and $Z^0\to\widetilde{W}\overline{\widetilde{W}}$ decays dominate when they are kinematically allowed: the chance that each of the two quarks forms an independent jet is small for the decay $W\to\widetilde{W}\widetilde{\gamma}$, $\widetilde{W}\to q\bar{Q}\widetilde{\gamma}$ when the $\widetilde{W}$ is light and fast moving. Unlike as in our earlier paper[24] where the dijet cross section was roughly flat from $m_{\widetilde{W}}\sim 50$ GeV to the kinematic limit, the dijet cross sections shown here falls off for large $\widetilde{W}$ masses. This is an effect of the more detailed trigger and selection criteria used in this paper.

Before turning our attention to the distributions, it is worthwhile to briefly mention the effects of the various triggers used in our calculation. For brevity, we discuss only the case for $Z^0\to\widetilde{W}\overline{\widetilde{W}}$ decays at $\sqrt{s}=630$ GeV. The results are summarized in Table II. We see that for heavier gauginos, the left-right trigger (5.3c) plays a substantial role since it allows jets with 15 GeV $<E_T<25$ GeV. Trigger (5.3b) is almost ineffectual for monojets (in our parton-model calculation) since it requires a $\not{p}_T$ exceeding 25 GeV from the 4σ cut and hence a jet of 25 GeV, i.e., such events would have been triggered by the jet E_T trigger (5.3a).

TABLE II. Effects of various triggers for hadronic events from $Z^0\to\widetilde{W}\overline{\widetilde{W}}$ decays at $\sqrt{s}=630$ GeV.

Trigger	$m_{\widetilde{W}}=25$ GeV	$m_{\widetilde{W}}=40$ GeV
jet$>$25 GeV	11.8 pb	8 pb
$E_T>80$ GeV	0.05 pb	1.7 pb
Left-right trigger	1.7 pb	4.0 pb

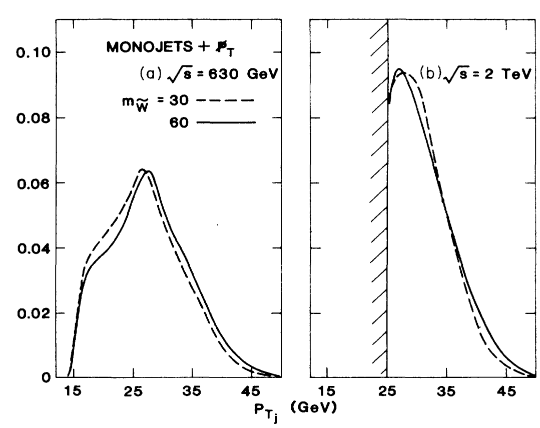

FIG. 11. Jet-p_T distributions in monojet events for the same parameters as in Fig. 10.

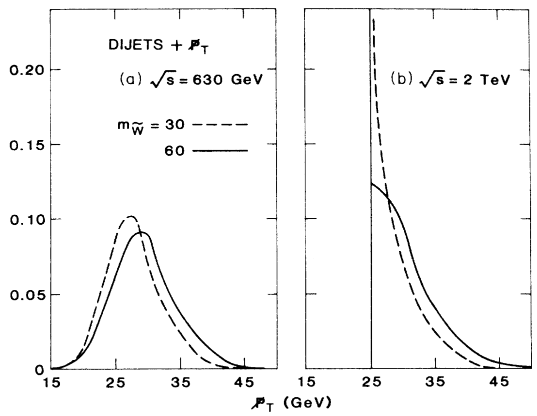

FIG. 12. Missing-p_T ($\not{p}_T$) distributions in dijet + $\not{p}_T$ events for the same parameters as in Fig. 10.

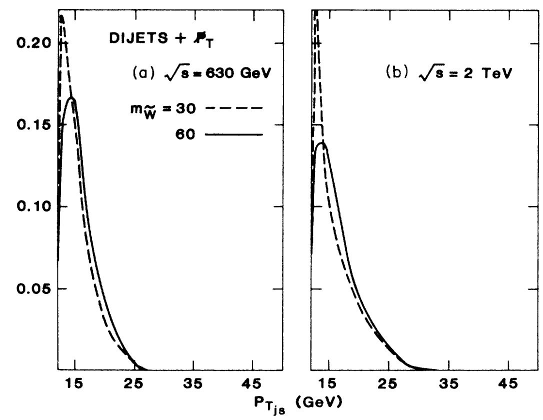

FIG. 14. p_T distribution of the slow jet in dijet + $\not{p}_T$ events for the same parameters as in Fig. 10.

The monojet + $\not{p}_T$ and dijet + $\not{p}_T$ cross sections are observable over a wide range of $\tilde{W}$ ($\tilde{Z}$) masses. Of course, standard-model backgrounds[47] to these events have to be thoroughly understood and subtracted from the data sample before any signal can be claimed.

Very recently, the UA1 Collaboration by an analysis of their monojet data, has announced[48] a limit $m_L > 41$ GeV (90% confidence level) on the mass of a new sequential heavy lepton. From our Monte Carlo analysis for the decay $W \to L\nu$, we find a cross section of 36 pb for monojets and 9 pb for dijets at $\sqrt{s} = 630$ GeV, assuming the same acceptance criteria discussed previously. From Fig. 8, a 36 pb monojet cross section corresponds to $m_{\tilde{W}} \gtrsim 40$ GeV.

We now turn to a study of the various distributions for the jet(s) + $\not{p}_T$ processes. The $\not{p}_T$ and $p_{T\text{jet}}$ distributions for the monojet events are shown in Figs. 10 and 11, for $m_{\tilde{W}} = 30$ and 60 GeV. We see that the $\not{p}_T$ distributions peak around 28 GeV and fall off to zero for $\not{p}_T \gtrsim 50$ GeV independent of $m_{\tilde{W}}$ and $\sqrt{s}$. The transverse momentum of the monojet peaks at a similar value as expected. The shoulder in the $p_{T\text{jet}}$ distribution is due to the left-right trigger (5.3c) which allows $\not{p}_T$ events with jet p_T between 15 GeV and 25 GeV to be accepted.

The $\not{p}_T$ distribution and p_T distributions of the fast and slow jets coming from the dijet + $\not{p}_T$ events are shown in Figs. 12, 13, and 14, respectively, for $m_{\tilde{W}} = 30$ and 60 GeV. For $m_{\tilde{W}} = 30$ GeV, the dominant sources of dijets are $W \to \tilde{W}\tilde{Z}$ and $Z^0 \to \tilde{W}\bar{\tilde{W}}$ processes whereas for $m_{\tilde{W}} = 60$ GeV the process $W \to \tilde{W}\tilde{\gamma}$ alone contributes. This results in a softer $\not{p}_T$ spectrum for the lower mass $\tilde{W}$ case. The p_T (fast jet) distribution for $m_{\tilde{W}} = 30$ GeV has a longer tail extending out to 50 GeV whereas that from the 60-GeV $\tilde{W}$ effectively cuts off below $p_T \simeq 45$ GeV. This is a reflection of the fact that in the $\tilde{W}\tilde{\gamma}$ case both jets come from the decay of a single parent; if one of the quarks was too hard the other quark would not be hard enough to be identified as a jet. The p_T distributions of the slow jet can be similarly understood.

Shown in Fig. 15 is the distribution of the azimuthal opening angle between the jets in dijet + $\not{p}_T$ events. We see that the distribution (at the CERN energy) for $m_{\tilde{W}} = 60$ GeV is intermediate between the $m_{\tilde{W}} = 30$ and 40 GeV cases. For $m_{\tilde{W}} = 30$ GeV, both $W \to \tilde{W}\tilde{Z}$ and $Z^0 \to \tilde{W}\bar{\tilde{W}}$ contribute with the gauginos carrying rather

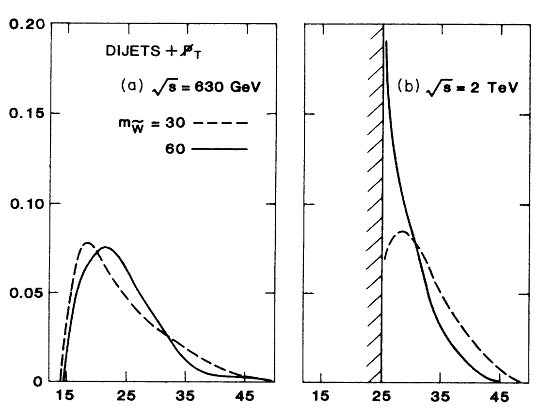

FIG. 13. p_T distribution of the fast jet in dijet + $\not{p}_T$ events for the same parameters as in Fig. 10.

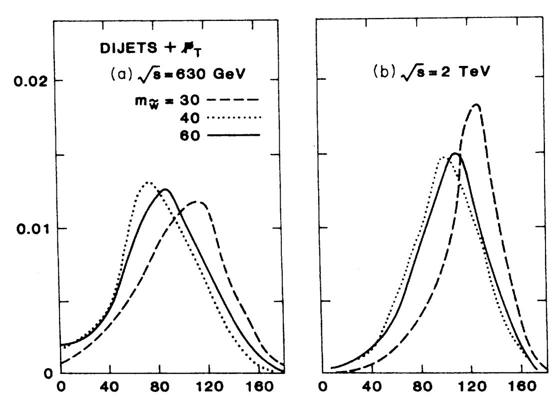

FIG. 15. Distribution in azimuthal opening angle ($\Delta\phi$) between dijets in dijet + $\not{p}_T$ events for the same parameters as in Fig. 10, except that the $m_{\tilde{W}} = 40$ GeV case is included here.

large transverse momenta causing the dijets to be more back to back. For $m_{\widetilde{W}}=40$ GeV, $Z^0 \to \widetilde{W}\overline{\widetilde{W}}$ dominates, but since the gauginos are slower moving greater acollinearity results. The $m_{\widetilde{W}}=60$ GeV case is kinematically different in that both jets come from the decay of a single particle. At Fermilab energies a similar trend is seen except that the $m_{\widetilde{W}}=40$ GeV and $m_{\widetilde{W}}=60$ GeV distributions are more similar. The differences between the two energies is a reflection of the different detector specifications used.

In summary, the hadronic decays of the gauginos lead to observable jet(s)$+\not{p}_T$ cross sections at both CERN and Fermilab energies. The total cross section exceeds 10 pb for $m_{\widetilde{W}} \lesssim 63$ GeV at CERN and for $m_{\widetilde{W}} \lesssim 70$ GeV at Fermilab. These values of $m_{\widetilde{W}}$ (particularly for the Tevatron) are dependent on the photino mass since we are in the vicinity of the kinematic end point for the $W \to \widetilde{W}\widetilde{\gamma}$ decay. We note that monojet cross sections dominate dijet cross sections over the range of $m_{\widetilde{W}}$ where the cross section is significant.

VI. MULTILEPTON SIGNALS FROM THE LEPTONIC DECAYS OF GAUGINOS

We now turn to a discussion of the signals resulting from the leptonic decays of both gauginos produced in the processes, $\bar{p}p \to \widetilde{W}^{\pm}\widetilde{Z}+X$ or $\bar{p}p \to \widetilde{W}\overline{\widetilde{W}}+X$. These processes could be a source of spectacular isolated multilepton-plus-$\not{p}_T$ events with minimal hadronic activity—only that associated with higher-order QCD corrections to W and Z production. Hence, these events are essentially free of standard-model backgrounds. We will postpone any discussion of single-lepton signatures to Sec. VIII since these have large standard-model backgrounds and because a different set of cuts is needed for the analysis of multilepton as opposed to single-lepton signatures. We have once again fixed the scalar-quark and scalar-lepton masses at 200 GeV and the photino mass at 8 GeV in our analysis. Our results are insensitive to these particular mass choices as long as the scalar fermions are heavier than the gauginos so that two-body decays of the gauginos are kinematically suppressed.[16] Also, we assume that the scalar-fermion masses are $\lesssim 300$ GeV so that the $\widetilde{Z} \to \widetilde{\gamma} f\bar{f}$ decay dominates the $\widetilde{Z} \to \widetilde{W} f \bar{F}$ decay (see Fig. 7).

In our analysis of the multilepton events, we require the following acceptance conditions for both CERN and Fermilab energies:

$$|p_{Te}| > 10 \text{ GeV}, \quad |\eta_e| < 3.0 \, , \qquad (6.1a)$$
$$|p_{T\mu}| > 3 \text{ GeV}, \quad |\eta_\mu| < 2.0 \, .$$

In addition, we require that at least one of the muons in any multilepton event be in the central region:

$$|\eta_\mu| < 1.3 \, . \qquad (6.1b)$$

Because we expect the multilepton signals to be very characteristic, we have not imposed any $\not{p}_T$ requirement on them. In addition, we have incorporated Gaussian resolution errors on the measurement of electron and muon momenta via the functions

$$\frac{\Delta E_e}{E_e} = \frac{0.15}{\sqrt{E_e}}, \quad |\eta_e| < 1.5 \, ,$$
$$= \frac{0.18}{\sqrt{E_e}}, \quad |\eta_e| > 1.5 \, , \qquad (6.2)$$
$$\Delta(1/p_\mu) = 0.005 \, ,$$

where E_e and p_μ are expressed in GeV.

We have been guided in our choice of acceptances and resolutions (6.1) and (6.2) by those used by UA1 Collaboration. We understand that the CDF will have an electron measurement at least comparable with that at UA1. However, since the muon detector is not expected to be completely installed, at least in the initial phase of the operation, one should view the signals with muons as indicative of the physics that would be possible to extract from the Tevatron data when the complete muon detector is functioning.

The trilepton cross sections for CERN and Fermilab Tevatron energies are shown in Fig. 16. These signals come only from the leptonic decay of both the $\widetilde{W}$ and $\widetilde{Z}$ when they are produced via $W \to \widetilde{W}\widetilde{Z}$. The signal thus cuts off at $m_{\widetilde{W}} + m_{\widetilde{Z}} = M_W$; the precise values of the $\widetilde{W}$ and $\widetilde{Z}$ masses at the cutoff point depend on $m_{\widetilde{\gamma}}$ (via the soft-SUSY-breaking gaugino mass μ_2).

One might have expected this signal to be small because of the small branching fraction for the leptonic decay of the $\widetilde{W}$. This may be compared to the case of light scalar fermions[16] in which $\widetilde{W} \to l\widetilde{\nu}$, $\widetilde{l}\nu$ and $\widetilde{Z} \to \widetilde{l}\bar{l}$ decays are dominant, with $\widetilde{l} \to l\widetilde{\gamma}$. In that case, some of the final-state leptons were soft and much of the trilepton signal could not pass the acceptance cuts. For the three-body decays we are considering, the final-state leptons tend to

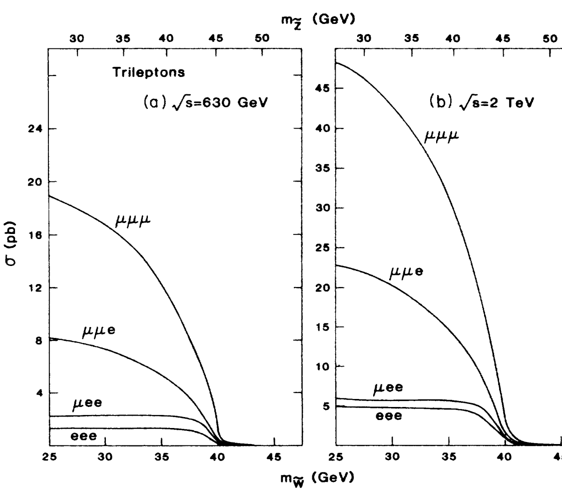

FIG. 16. Expected trilepton cross sections from $W \to \widetilde{W}\widetilde{Z}$ when both $\widetilde{W}$ and $\widetilde{Z}$ decay leptonically. The cuts are as described in Sec. VI of the text for (a) $\sqrt{s}=630$ GeV and (b) $\sqrt{s}=2$ TeV and $m_{\widetilde{\gamma}}=8$ GeV.

share the momentum equally; the resulting increase in the fraction of events that pass the cuts (particularly for μ) makes up for the reduced branching fraction.

The ordering of the signals is just a reflection of the difference in p_T cuts on the e and μ. It is clear from the difference in the e and μ cross sections that the effect of the p_T cut is very large and hence, the importance of being able to measure isolated electrons in multilepton events to $p_{Te} \simeq 5$ GeV at the Tevatron cannot be overemphasized.

The trimuon cross section roughly follows the gaugino production cross section, whereas the trielectron cross section is flat up to the phase-space boundary. This is because heavier gauginos are more likely to produce harder electrons which pass the p_{Te} cut; the reduction in the $\tilde{W}\tilde{Z}$ cross section with increasing $\tilde{W}$ mass is compensated for by the increase in mean p_T of the final-state leptons. Because the p_T acceptance cut on the muons in only 3 GeV as compared to 10 GeV for electrons, this effect is relatively unimportant for the trimuon signal.

We now turn to a discussion of the dilepton + $\not{p}_T$ cross sections shown in Figs. 17—19. These come from the leptonic decays of the $\tilde{W}$ and $\tilde{Z}$ in $\tilde{W}\bar{\tilde{W}}$ and $\tilde{W}\tilde{Z}$ events, where $\tilde{W}\tilde{Z}$ gives dileptons when one of the three leptons fails to pass the acceptance cuts. Therefore, a third of the $\tilde{W}\tilde{Z}$ dilepton events have the same-sign dileptons. The following features of the curves are worth noting.

(i) The number of dilepton events from $Z \rightarrow \tilde{W}\bar{\tilde{W}}$ is smaller than those from $W \rightarrow \tilde{W}\tilde{Z}$; this is just a reflection of the relative sizes of the W and Z cross sections. We note that the dilepton cross section from $\tilde{W}$ pairs is nearly flat up to the phase-space boundary.

(ii) Since the muons are more likely to pass the p_T cut (and so, are harder to miss), same-sign $e\mu$ events which come from $\tilde{W} \rightarrow \mu$, $\tilde{Z} \rightarrow e^+e^-$ outnumber same-sign dimuon events from $\tilde{W} \rightarrow \mu$, $\tilde{Z} \rightarrow \mu^+\mu^-$. The same-sign dielectron events occur only when the $\tilde{W}$ and $\tilde{Z}$ both decay into electrons. It is interesting to see that the rate for $e^-e^- + e^+e^+$ pairs exceeds the e^+e^- production rate from $\tilde{W}$ pairs as shown in Fig. 19.

At this point, we note that we have assumed that 100% of the leptons within our acceptance are detected. This is, of course, not the case with a real detector and a complete detector simulation must include this. We can, however, qualitatively discuss the effect of incorporating detection efficiency into our calculation. Consider for example, trimuon events and assume that muons cannot be detected if they are within 20° (in azimuth) of the vertical. For any one muon, this gives an overall factor of $\frac{7}{9}$ on its probability of detection. For $\tilde{W}$'s and $\tilde{Z}$'s that are relatively slow moving, it is a good approximation to assume that the azimuthal directions of the three muons are uncorrelated. In this case, it is straightforward to check that 47% of the trimuon events survive, 13.4% become same-sign dimuons, 26.9% opposite-sign dimuons, 11% single muons, and 1.1% are lost. In practice, however, because of the motion of the gauginos, the directions of the three

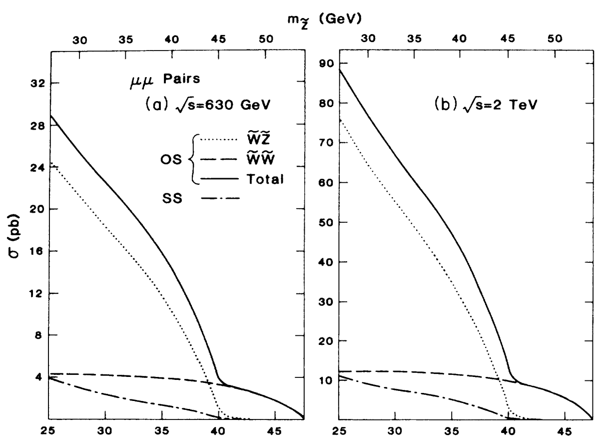

FIG. 17. Expected dimuon cross sections from the leptonic decays of gauginos. The parameters are as in Fig. 16. We present curves for opposite-sign (OS) and same-sign (SS) dimuons.

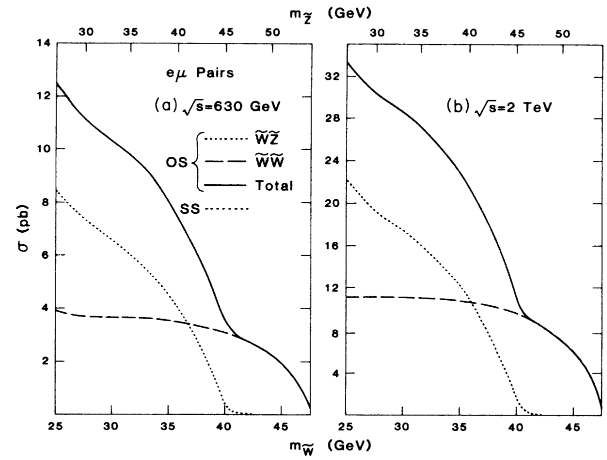

FIG. 18. Expected $e\mu$ cross sections from the leptonic decay of gauginos. The parameters are as in Fig. 16. Note that $\tilde{W}\tilde{Z}$ production gives the same number of opposite-sign and same-sign lepton pairs.

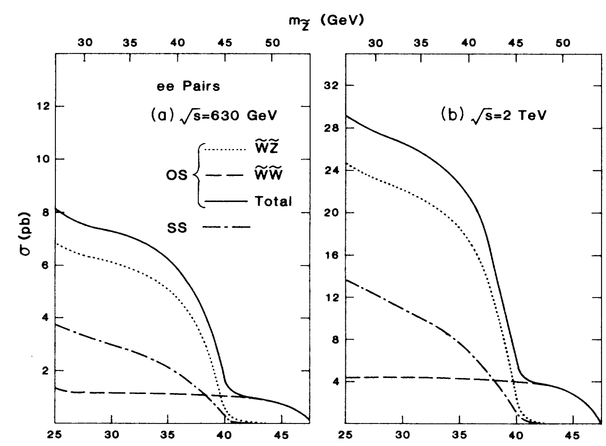

FIG. 19. Expected dielectron cross sections from the leptonic decay of gauginos. The parameters are as in Fig. 16.

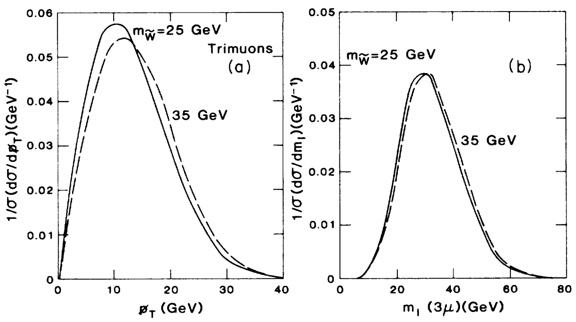

FIG. 20. Distribution in (a) missing p_T and (b) trimuon invariant mass for trimuon events from gaugino pairs for $m_{\tilde{W}}=25$ and 35 GeV, and $m_{\tilde{\gamma}}=8$ GeV. The distributions are normalized to unity, and are virtually the same for $\sqrt{s}=630$ GeV as for $\sqrt{s}=2$ TeV.

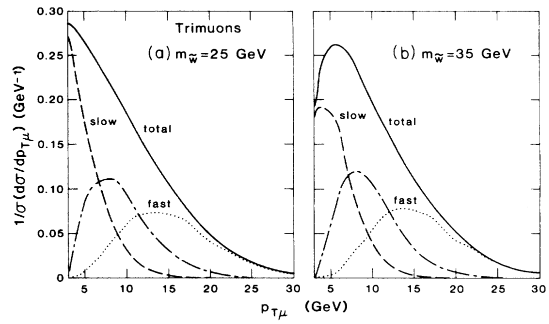

FIG. 22. Expected distribution of muon p_T from trimuon events when $W\to\tilde{W}\tilde{Z}$, for (a) $m_{\tilde{W}}=25$ GeV and (b) $m_{\tilde{W}}=35$ GeV.

leptons are in general correlated and thus we expect the above numbers to be somewhat altered. We expect that the modification due to such correlations is not too large for heavy enough gauginos. We must emphasize that in our simplified example only 12% of the trimuon events were either lost or became part of the (background-contaminated) single-lepton sample. Thus, in spite of corrections due to detection efficiency, we believe that there will be a substantial number of background-free multilepton + $\not{p}_T$ events from the decay of gauge bosons into gaugino pairs.

Various distributions from the largest trilepton and dilepton signals are shown in Figs. 20–24. There is little difference other than normalization between the distributions of transverse or Lorentz-invariant quantities at CERN and Tevatron energies. This is a reflection of the fact that in both cases the gauginos are produced dominantly by the decay of gauge bosons and that we have used the same set of cuts for both cases.

We see from Figs. 20 and 21 that although the $\not{p}_T$ distributions for $\mu\mu\mu$ and $e\mu\mu$ events extend out to beyond 30 GeV, most of the events have $\not{p}_T$ between 5 and 20 GeV. We again emphasize that these isolated multilepton events are spectacular and should be easy to identify even though $\not{p}_T$ in these events is rather low. Also shown in these figures is the invariant mass of the trimuons [Fig. 20(b)] and the p_T and invariant-mass distribution of the dimuons in $e\mu\bar{\mu}$ events [Figs. 21(b) and 21(c)]. Since the μ pairs in $e\mu\bar{\mu}$ events necessarily come from the decay of a $\tilde{Z}$, we have $m_I(\mu\mu)<m_{\tilde{Z}}-m_{\tilde{\gamma}}$, and, hence, a study of the upper endpoint of this distribution can yield information about the gaugino masses. We see that increasing the $\tilde{W}$ ($\tilde{Z}$) mass makes all the distributions harder except the p_T ($\mu\bar{\mu}$) distribution in $e\mu\bar{\mu}$ events.

The p_T spectra of the three muons in the trimuon events are shown in Fig. 22 for $m_{\tilde{W}}=25$ GeV and $m_{\tilde{W}}=35$ GeV. The spectra are only slightly harder in the case of the heavier gauginos. It may be of interest to compare these with the momentum distribution of the trimuon events in the data of the UA1 Collaboration.

We now turn our attention to $\mu\bar{\mu}$ and $e\mu$ events. The invariant mass, $\not{p}_T$ and azimuthal opening angle ($\Delta\phi$) distributions are shown in Figs. 23 and 24. As can be seen from Figs. 17 and 18, for $m_{\tilde{W}}=30$ GeV, $\tilde{W}\tilde{Z}$ is the dominant source of dileptons while for $m_{\tilde{W}}=40$ GeV, all the events are from $\tilde{W}$ pairs. This is the reason why the invariant-mass distribution for dimuons is so much softer for $m_{\tilde{W}}=30$ GeV than that for $m_{\tilde{W}}=40$ GeV. The dimuons from $\tilde{W}\tilde{Z}$ events are mostly from $\tilde{Z}\to\mu\bar{\mu}$, $\tilde{W}\to e$ with the electron being lost and hence their invariant-mass distribution [Fig. 23(a)] is governed by the $\tilde{Z}$ mass. [Note that it closely resembles the $m_I(\mu\bar{\mu})$ distribution from $e\mu\bar{\mu}$ events for $m_{\tilde{W}}=25$ GeV shown in Fig. 21.] The invariant-mass distribution of $e\mu$ pairs is

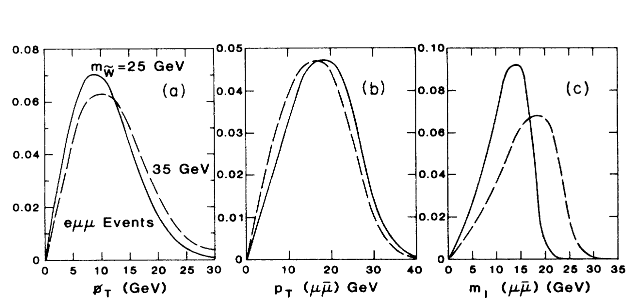

FIG. 21. Distributions from $e\mu\mu$ events for (a) missing p_T, (b) p_T of dimuon pair, and (c) invariant mass of dimuon pair for $m_{\tilde{W}}=25$ GeV (solid lines) and $m_{\tilde{W}}=35$ GeV (dashed lines). The plots are normalized to unity; absolute magnitudes can be read off from Fig. 16.

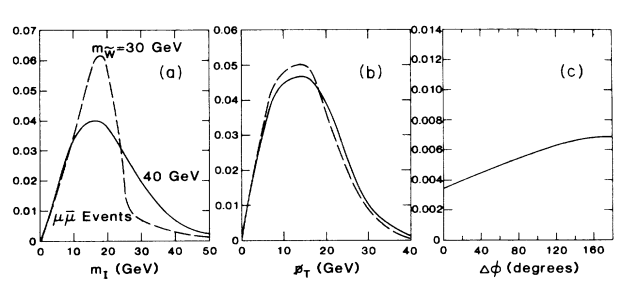

FIG. 23. Distributions from $\mu\bar{\mu}$ events from gauginos for (a) dimuon invariant mass, (b) missing p_T, and (c) azimuthal opening angle. The plots are for $m_{\tilde{W}}=30$ GeV (dashed lines) and $m_{\tilde{W}}=40$ GeV (solid lines). In (c), the two curves are virtually the same.

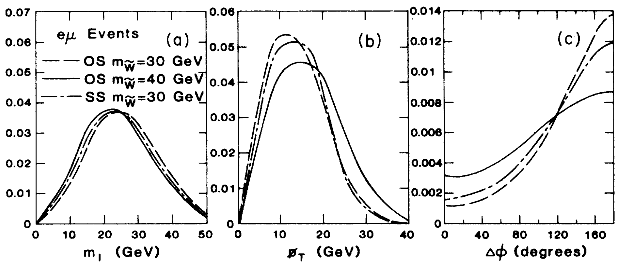

FIG. 24. Distributions from $e\mu$ events for (a) dilepton invariant mass, (b) p_T missing, and (c) azimuthal opening angle. The plots are for $m_{\tilde{W}}=30$ GeV (opposite sign, dashed line; same sign, dotted-dashed line) and $m_{\tilde{W}}=40$ GeV (opposite sign only allowed, solid line).

harder than that for dimuons partly due to the higher-p_T cut on e and partly due to the fact that the e and μ come from different gauginos. The $\not{p}_T$ distributions are similar for both $e\mu$ and $\mu\mu$ events and they both are harder than the $\not{p}_T$ distribution for trilepton events—this is because the photinos tend to be hard in events where one lepton is soft and/or more particles are carrying off missing p_T.

The $\Delta\phi$ distributions are quite different for $\mu\mu$ and $e\mu$ events. We see from Fig. 23(c) that the $\Delta\phi$ distribution is flat for $\mu\bar{\mu}$ events and hence there is a large fraction of acollinear $\mu\bar{\mu}$ pairs. For the $e\mu$ case shown in Fig. 24(c), the distribution for $m_{\tilde{W}}=40$ GeV (all from $\tilde{W}\bar{\tilde{W}}$) is flattest reflecting the fact that their parent $\tilde{W}$ have rather low p_T. For $m_{\tilde{W}}=30$ GeV, the opposite-sign (OS) $e\mu$ pairs (dashed curve) are more back to back than the same-sign (SS) $e\mu$ pairs (dotted-dashed curve). This is because the latter (SS) come only from $\tilde{W}\tilde{Z}$ events whereas a third of the former (OS) events come from $Z\to\tilde{W}\bar{\tilde{W}}$ decays.

We remark here that if such multilepton events are observed, information on gaugino masses can also be obtained by confronting the various event topologies with those of Figs. 16—19. For instance, if acollinear, opposite-sign $e\mu$ and $\mu\mu$ pairs are observed but no trilepton or same-sign dileptons are seen, one can conclude $M_W<m_{\tilde{W}}+m_{\tilde{Z}}$ and $m_{\tilde{W}}<M_Z/2$.

To conclude, if the decays $W\to\tilde{W}\tilde{Z}$ and $Z^0\to\tilde{W}\bar{\tilde{W}}$ are both kinematically accessible, there is a large rate for background-free multilepton-plus-$\not{p}_T$ events that are essentially free of hadronic activity. For $m_{\tilde{W}}=38$ GeV, and assuming 100% detection efficiency we expect 13 pb of trilepton-plus-$\not{p}_T$ events, 19 pb of opposite-sign dilepton-plus-$\not{p}_T$ events, and 4 pb of same-sign dilepton-plus-$\not{p}_T$ events. This does not include multilepton events when one of the gauginos decays hadronically and the other leptonically. Such events will be studied in the next section.

VII. JET-PLUS-LEPTON SIGNALS FROM THE DECAY OF GAUGINOS

In the last two sections we have considered the signals resulting from the hadronic or leptonic decays of both $\tilde{W}$ and $\tilde{Z}$. Here, we consider the possibility that one of the gauginos decays leptonically and the other hadronically. This would lead to jet(s) + (multi)lepton + $\not{p}_T$ events.[17,22–24] Such topologies are also expected in the standard model, particularly from the leptonic decay of heavy flavors.[49] Nevertheless, these events are important since if gauginos can indeed be produced at hadron colliders, these mixed signals *must* be present in a definite proportion to the jet(s) + $\not{p}_T$ and the multilepton signals discussed in Secs. V and VI, respectively. Thus, if light gauginos exist, a definite excess of jet(s) + lepton(s) + $\not{p}_T$ signals over and above that expected from the standard model is predicted.

In our computation of the cross sections for these mixed signals, we have required that these events have a minimum $\not{p}_T$ and that the $\not{p}_T$ vector should be isolated as discussed for purely hadronic signals in Sec. V. We have also used the same acceptance[50] for jets and leptons as described in Secs. V and VI for the single lepton + jet(s) + $\not{p}_T$ events. In this case, we also require

$$|p_{Te}|>\begin{cases}15\text{ GeV (CERN)},\\10\text{ GeV (Fermilab)},\end{cases}\tag{7.1a}$$

$$|p_{T\mu}|>8\text{ GeV},\tag{7.1b}$$

in addition to the acceptance of Eq. (6.1) in Sec. VI.

We have also required an isolation cut on the electrons at CERN energies, i.e., we require that an electron be identified only if all partons within $\Delta r=1$ of the electron momentum satisfy

$$|p_{Te}|>4\,|p_{T\,\text{parton}}|\ .\tag{7.2}$$

Whenever an electron fails to satisfy this requirement, we assume that it cannot be distinguished from a hadron, and hence, treat it as part of the jet. We have also assumed that all the muons within the acceptance are identified, both at CERN and Fermilab energies. For the CDF, because of its vastly improved segmentation as compared to UA1, we assume that all the electrons (even if close to a parton) can be identified. We again caution the reader that we have assumed complete ($\eta<4$) muon detection at the Tevatron, even though this will not be the case in the

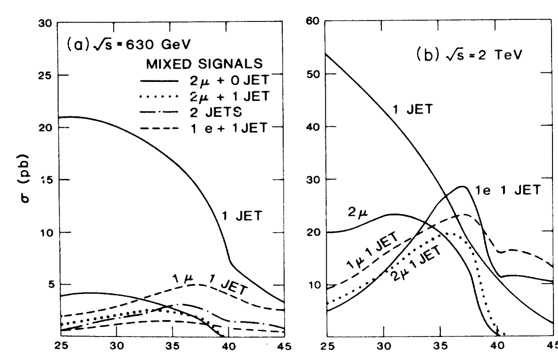

FIG. 25. Topological cross sections from gaugino production ($\tilde{W}\bar{\tilde{W}}$ and $\tilde{W}\tilde{Z}$) where one gaugino decays leptonically and one hadronically. The plots are for (a) $\sqrt{s}=630$ GeV and (b) $\sqrt{s}=2$ TeV, using the acceptance cuts given in Secs. V—VII in the text. We show only the largest cross sections in the figure.

initial phase of its operation.

For the mixed signals, an event may either be triggered by a hard lepton [Eqs. (7.1) and (7.2)] or by any of the jet triggers [(5.3a—5.3c)] discussed in Sec. V. The resulting cross sections for various topologies with the largest cross section are shown in Fig. 25 for both CERN and Fermilab energies. The curves labeled 1 jet (or 2 jets) denote those events where the lepton(s) are either outside the acceptance or misidentified as hadrons. This cross section should be added to the monojet (dijet) cross section discussed in Fig. 8 (9) and Sec. V. We make the following remarks concerning these signals.

(i) The dominant n jet + m lepton + $\not{p}_T$ signal turns out to be the one for $m=0$, and $n=1$, i.e., monojets. In the final analysis, these rates should be added to the monojet cross sections of Fig. 8; we keep them separate here because of their different origin. Also presented in Fig. 25 are dijet events with undetected leptons. These dijet rates are much smaller than the corresponding monojet rates because in this case both jets must come from the same gaugino. The dijet signal for $\sqrt{s}=2$ TeV is tiny (~ 1 pb), and is not included in Fig. 25(b); the reasons dijets are at all substantial at $\sqrt{s}=630$ GeV is due to the stricter electron cuts (there is more chance of an electron being misidentified as a hadron) and also because the events can be triggered by the scalar E_T and left-right triggers in our simulation.

(ii) All rates for events containing a single identifiable lepton ($m=1$) are less than 5 pb over the whole range of $\widetilde{W}$ masses at $\sqrt{s}=630$ GeV. In this class of events the single leptons should be hard and isolated. However, these signals may compete with those from heavy-flavor backgrounds. The single leptons + jet signals at $\sqrt{s}=2$ TeV are much larger than the corresponding CERN signals due to the more liberal acceptance conditions. In this case, however, the heavy-flavor backgrounds are likely to be much larger also. The sharp kinks in the 1 lepton + 1 jet curves at $\sqrt{s}=2$ TeV come from the cutoff of the $\widetilde{W}\widetilde{Z}$ cross section and from the fact that the 1 lepton + 1 jet signal from $\widetilde{W}\widetilde{Z}$ is quite large up to the edge of the kinematic boundary for $Z^0 \to \widetilde{W}\overline{\widetilde{W}}$.

(iii) The muon + jet signals which come from both $\widetilde{W}\widetilde{Z}$ and $\widetilde{W}\overline{\widetilde{W}}$ are significant at both CERN and Fermilab energies. At CERN, the more stringent cuts on the electron reduces the $1e+1$ jet signal relative to the $1\mu+1$ jet signal. We also see that the $2\mu+1$ jet signal is large. This is due to the greatly increased acceptance in p_T ($p_{T\mu} \geq 3$ GeV) for the dimuons. For electrons, there is no such increase in acceptance. This is also the reason why the $1e+1$ jet signal at the Tevatron exceeds the $1\mu+1$ jet signal for intermediate values of $m_{\widetilde{W}}$: much of the n muon + m jet + $\not{p}_T$ signal manifests itself as dimuons plus jets whereas the n electron + m jet + $\not{p}_T$ signal is manifested mainly as a single electron + jets. For the largest $\widetilde{W}$ masses considered here, the $2e$ +jet signal reaches about 1.5 pb at $\sqrt{s}=2$ TeV.

(iv) There is a good chance of observing gauginos via the decay modes $\widetilde{Z} \to \mu\bar{\mu}\widetilde{\gamma}$ and $\widetilde{W} \to q\bar{Q}\widetilde{\gamma}$ when the decay $W \to \widetilde{W}\widetilde{Z}$ is allowed. The rate for dimuon plus 0 or 1 jets at CERN exceeds 5 pb for $m_{\widetilde{W}} < 35$ GeV. These events should consist of two isolated muons along with jet activity, so backgrounds from $b\bar{b}$, $c\bar{c}$, etc., will be small. The dimuon plus 0 or 1 jet signal at the Tevatron is about 30 pb for $m_{\widetilde{W}} < 35$ GeV; this reflects not only the increased W-production cross section at the Tevatron, but also the wider muon rapidity acceptance which we have allowed. These dimuon events with jet activity must also be taken into account in the search for acollinear dimuons discussed in Sec. VI, but unlike in those events, there is a considerable amount of hadronic activity from the decay products of the $\widetilde{W}$.

To summarize, the mixed decays (one hadronic, the other leptonic) of the $\widetilde{W}$'s and $\widetilde{Z}$'s lead to a substantial amount of jet(s) + lepton + $\not{p}_T$ signals. At $\sqrt{s}=630$ GeV, this signal exceeds 25 pb for $m_{\widetilde{W}} \leq 37.5$ GeV, whereas at Tevatron energies, the corresponding signal exceeds 100 pb. It is also interesting to note that $1e+1$ jet + $\not{p}_T$ and $1\mu+1$ jet + $\not{p}_T$ signals for $\sqrt{s}=2$ TeV each exceed 10 pb for $\widetilde{W}$ masses as high as 45 GeV. Signatures involving one lepton + jet(s) + $\not{p}_T$ will, however, be less striking because they can also come from heavy-flavor production.

VIII. SINGLE-LEPTON SIGNALS FROM LEPTONIC DECAYS OF THE GAUGINOS

We have seen that if the decays $W \to \widetilde{W}\widetilde{Z}$ and $Z^0 \to \widetilde{W}\overline{\widetilde{W}}$ are kinematically accessible, there can be a large cross section for essentially background-free multilepton events which would then serve as characteristic signatures for gauginos. We now consider the possibility that $\widetilde{W}$ and $\widetilde{Z}$ are so heavy that the only allowed decay of a gauge boson into gauginos that is kinematically allowed is $W \to \widetilde{W}\widetilde{\gamma}$. The hadronic decay of the gaugino leads to monojet (dijet) events as has been discussed in Sec. V. Here, we consider the possibility of studying the leptonic decay $\widetilde{W} \to l\bar{\nu}\widetilde{\gamma}$ of the $\widetilde{W}$ which leads to single lepton + $\not{p}_T$ events.

Shown in Fig. 26 are the p_T and $\cos\theta$ distributions of the emerging electron (θ is the angle between the outgoing electron and the incoming proton). The distributions for the muon are identical except for differences in resolution

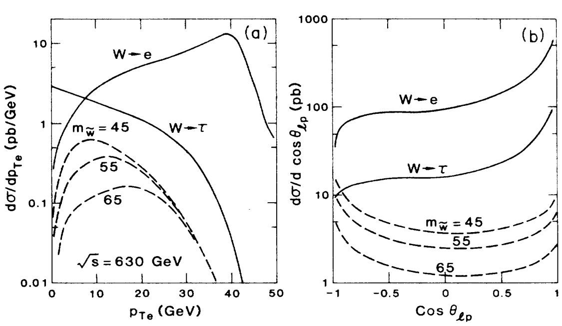

FIG. 26. Distribution of (a) p_{Te} and (b) $\cos\theta_{l,p}$ in the $p\bar{p}$ c.m. frame for $\sqrt{s}=630$ GeV for the SUSY signal from $W \to \widetilde{W}\widetilde{\gamma}$; $\widetilde{W} \to e\bar{\nu}\widetilde{\gamma}$ for $m_{\widetilde{W}}$=45, 55, and 65 GeV. Also shown are the background contributions from $W \to e\bar{\nu}$ and $W \to \tau\bar{\nu}$; $\tau \to e\nu\bar{\nu}$. The backgrounds overwhelm the signal. The same is true for $\sqrt{s}=2$ TeV.

smearing for the electron and the muon. Also shown are the standard-model contributions from $W \to e\bar{\nu}$ and $W \to \tau\bar{\nu} \to l\nu\bar{\nu}\bar{\nu}$. It is clear that the backgrounds overwhelm the signal for almost the whole of the phase space; i.e., there is no set of cuts we can use that will enhance the signal to background ratio up to ~ 1. This situation is unchanged for Tevatron energies.

We conclude that if $m_{\tilde{W}} \gtrsim 45$ GeV, one will have to rely on the hadronic decay of the $\tilde{W}$ for any observable signal. As has been already mentioned, there are several standard-model backgrounds that need to be evaluated before one can conclude the presence of a signal. The $\tilde{W}$ search would then closely parallel a sequential heavy-lepton search.[51] The nonresonant production of heavy $(2m_{\tilde{W}} > M_Z)\tilde{W}$ and $\tilde{Z}$ is small as may be expected (see Fig. 2) and hence it is unlikely that multilepton signals from this source would lead to the identification of gauginos at either the CERN collider or the Fermilab Tevatron. In this case, the dominant production mechanism for $\tilde{W}$ and $\tilde{Z}$ may well be through scalar-quark and gluino production, with their subsequent decay to gauginos.[52]

IX. A STUDY OF THE MODEL DEPENDENCE: VARIATION OF v'/v

In Sec. II we have seen that the gauge-Higgs-fermion sector of all two-Higgs-doublet models could be conveniently parametrized in terms of the $\tilde{W}$ mass, the photino mass, and the ratio v'/v of the Higgs-field vacuum expectation values. Thus, given a value of v'/v, all cross sections can be calculated as functions of just the SUSY-particle masses making it possible to obtain limits on their masses if there is no signal. As yet, our considerations have focused on the class of models that have $v'/v = 1$. In this section, we discuss the effect on the gaugino signal of relaxing this constraint. From the discussion in Sec. II, it is clear that altering v'/v changes the mixings in the gauge-Higgs-fermion system and also the masses in both the gaugino and scalar-fermion sectors. We discuss the effect of each separately.

For v'/v substantially different from unity, the decay $W \to \tilde{W}\tilde{Z}$ is not considered here for reasons discussed in Sec. II. This leaves open for investigation the channels $W \to \tilde{W}\tilde{\gamma}$ and $Z^0 \to \tilde{W}\bar{\tilde{W}}$. (As discussed in Sec. II, we do not consider the decays of the gauge bosons into Higgs-fermion states since these are more model dependent.) For small values of $m_{\tilde{\gamma}}$, Eq. (2.13c) is unaltered and as before, our results for $\tilde{W}\tilde{\gamma}$ ($\tilde{W}\bar{\tilde{W}}$) production via W (Z^0) decays can again be expressed in terms of $m_{\tilde{W}}$ [Eq. (2.6)]. The scalar-fermion masses enter the computation of the $\tilde{W}$ branching ratios. For $v'/v = 1$, the scalar quarks and scalar leptons are approximately degenerate and the branching fractions have a simple form.[43] If $v'/v \neq 1$, but the scalar fermions are all very heavy ($\gg M_W$), the branching fractions are governed by the decay via a virtual W boson, and hence, insensitive to any particular choice of scalar-fermion masses. For the branching ratio to be substantially affected, we need some of the scalar fermions much lighter than the others. Of particular interest is the case when the scalar neutrino is relatively light but the scalar electron and scalar quarks are all heavy so that the only allowed two-body decay mode of the $\tilde{W}$ is $\tilde{W} \to l\tilde{\nu}$. The presence of such a scalar neutrino would have escaped experimental detection.[35,36]

From Eqs. (2.18), it follows that this can be readily achieved if $v'/v < 1$. In the class of models we are considering, v'/v cannot be made arbitrarily small since the $\tilde{W}$ mass would then necessarily be smaller than the experimental bound $m_{\tilde{W}} \gtrsim 22$ GeV (Ref. 53). The allowed range of v'/v also depends on $m_{\tilde{\gamma}}$. Here, for the purposes of illustration, we choose $v'/v = 0.5$, $m_{\tilde{\gamma}} = 10$ GeV, and a scalar-neutrino mass of 10.8 GeV. The $\tilde{W}$ mass is then bounded above by $\simeq 52$ GeV whereas all the other scalar fermions [see Eq. (2.18)] have masses exceeding 51 GeV, i.e., the $\tilde{W}$ decays only via $\tilde{W} \to l\tilde{\nu}$.

Before proceeding to show the various topological cross sections from $Z \to \tilde{W}\bar{\tilde{W}}$, we note that for $v'/v \neq 1$, the mixing angles and hence the branching fraction for $Z^0 \to \tilde{W}\bar{\tilde{W}}$ is altered. Typically, this is reduced from its value with $v'/v = 1$. For example, for $v'/v \approx 0.23$, and a $\tilde{W}$ mass of about 30 GeV, the $Z \to \tilde{W}\bar{\tilde{W}}$ width is reduced by almost 40%. Although this reduces the total $\tilde{W}\bar{\tilde{W}}$ cross section, the 100% branching fraction for $\tilde{W}$ decay into the $l\tilde{\nu}$ mode provides dilepton-plus-$\not{p}_T$ signals from $\tilde{W}\bar{\tilde{W}}$ production at a greatly increased rate.

The cross section for the various topologies for $v'/v = 0.5$ and $m_{\tilde{\nu}} = 10.8$ GeV is shown as a function of $m_{\tilde{W}}$ at CERN and Fermilab Tevatron energies in Fig. 27. The cuts used are the same as those for the multilepton signals discussed in Sec. VII. The following features are worth noting.

(i) The large cross sections are due to the 100% leptonic branching fraction for the $\tilde{W}$.

(ii) Because the scalar-neutrino mass is only 10.8 GeV,

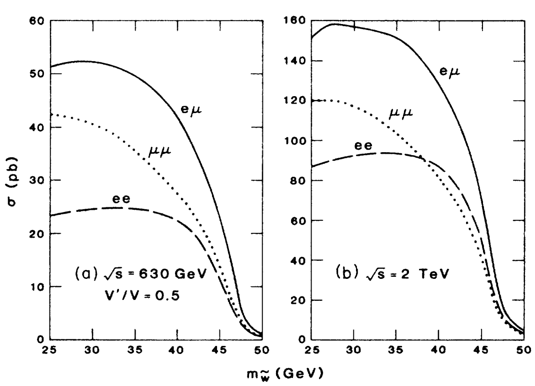

FIG. 27. Topological cross sections from gauginos when the ratio of two Higgs-field vacuum expectation values $v'/v = 0.5$. In this case, $W \to \tilde{W}\tilde{Z}$ is disallowed; however, $Z \to \tilde{W}\bar{\tilde{W}}$ is allowed, and $\tilde{W} \to l\tilde{\nu}$ where $l = e, \mu$ or τ with a branching fraction of 100%. In this figure, $m_{\tilde{\gamma}} = 10$ GeV and $m_{\tilde{\nu}} = 10.8$ GeV. All other SUSY-particle masses are greater than 50 GeV [see Eq. (2.18)].

substantially more electron events pass the cut increasing the proportion of ee and $e\mu$ events relative to the $\mu\mu$ events. It is interesting to compare this to the case of light scalar leptons with $v'/v=1$ considered in Ref. 16. It is clear that increasing the mass of the scalar neutrino will substantially decrease the number of electron events passing the cuts, but nevertheless it is important to note that the $Z^0 \to \widetilde{W}\overline{\widetilde{W}}$ mode provides an excellent way to search for $\widetilde{W}$ in the class of models in which the scalar neutrino is light.

(iii) Unlike in Sec. VI, the $e\mu$ decay mode is larger than the $\mu\mu$ decay mode because of the increased hardness of the electron p_T spectrum and the additional combinatorial factor of 2.

In this section, we have not studied the signal from $W \to \widetilde{W}\widetilde{\gamma}$ since for most of the allowed choice of $m_{\widetilde{W}}$ the signal from $Z^0 \to \widetilde{W}\overline{\widetilde{W}}$ is accessible. We remark here that because of the lightness of the scalar neutrino, the lepton would be relatively hard and hence the signal may be difficult to disentangle from the $W \to l\bar{\nu}$ and $W \to \tau\bar{\nu} \to l\nu\bar{\nu}$ background.

Finally, we briefly remark on the possibility $v'/v > 1$. In this case, r [in Eq. (2.18)] is negative and the lightest scalar fermion is $\widetilde{d}_L$ (for $m_{\widetilde{\gamma}} \approx 0$). Requiring that this be heavier than ~ 50 GeV so that there are not too many jet(s)-plus-$\not{p}_T$ events at the CERN collider, we find that all the scalar fermions are heavy leading approximately to the sort of branching fractions considered for the $v'/v=1$ case.[54]

In summary, we note that in the class of models with a light scalar neutrino, the $\widetilde{W}$ mass is expected to be small so that the decay $Z^0 \to \widetilde{W}\overline{\widetilde{W}}$ is almost always accessible. We find large cross sections for clean dilepton-plus-$\not{p}_T$ events (the rates for these would be sensitive to $m_{\widetilde{\nu}}$). It is important to note that the $\mu\bar{\mu}+\not{p}_T$ cross section at CERN (Tevatron) energies, assuming 100% detection efficiency exceeds 10 pb for $m_{\widetilde{W}} < 46$ GeV (48 GeV). This value is likely to be insensitive to $m_{\widetilde{\nu}}$ (except when $m_{\widetilde{\nu}} \simeq m_{\widetilde{W}}$) because of the low cut on the muon p_T. We therefore conclude that for the case $m_{\widetilde{l}}$, $m_{\widetilde{q}} > m_{\widetilde{W}} > m_{\widetilde{\nu}}$, it would be possible to substantially improve the current $\widetilde{W}$ mass limit $m_{\widetilde{W}} \gtrsim 22$ GeV obtained from the DESY PETRA data.

X. SUMMARY AND CONCLUDING REMARKS

We have performed a detailed analysis of the signals resulting from the decay of the $\widetilde{W}$ and $\widetilde{Z}$ [the mass eigenstates of the gauge-Higgs-fermion system that contain substantial SU(2)-gaugino components] at both CERN $Sp\bar{p}S$ and Fermilab Tevatron energies. Our analysis is fairly model independent in that we have examined a minimal SUSY model with general soft-supersymmetry-breaking terms (induced via the super-Higgs mechanism). In our study, we have assumed that the photino is light ($\lesssim 10$ GeV) and escapes detection. For a given photino mass, the gauge-Higgs-fermion mixing parameters depend (apart from $m_{\widetilde{W}}$) only on the ratio (v'/v) of the Higgs-field vacuum expectation values. We have taken v'/v to be unity throughout most of this paper, a value favored by many models.[19] All the SUSY-particle masses, couplings, and mixing parameters (except for the heavy-flavor sector which does not concern us in this paper) are determined in terms of $m_{\widetilde{\gamma}}$, $m_{\widetilde{W}}$, v'/v, and m_0, the common scalar-fermion mass at the unification scale (see Sec. II). The signatures are relatively insensitive to any particular values of these parameters except when one (or more) of the scalar fermions becomes lighter than $m_{\widetilde{W}}$ or $m_{\widetilde{Z}}$, thereby altering the decay patterns of the gauginos. In order to illustrate this, we have also studied the case $v'/v=0.5$ where the scalar neutrino can be light so that $\widetilde{W} \to l\widetilde{\nu}$ and $\widetilde{Z} \to \nu\widetilde{\nu}$ decays dominate the three-body decays $\widetilde{V} \to f\bar{F}\widetilde{\gamma}$ ($f,F=$quark or lepton).

In our analysis, we have attempted to model the UA1 detector acceptances and trigger requirements for $\sqrt{s}=630$ GeV. We have, however, made no attempt to simulate the exact trigger conditions, e.g., we have not varied trigger conditions according to their appropriate running times. The effects of the various triggers for the jet(s) + $\not{p}_T$ events are briefly indicated in Table II and discussed in Sec. V. We should also mention that we have not included hadronization effects and have assumed 100% detection efficiency for particles within the acceptance. For $\sqrt{s}=2$ TeV, we have attempted to model the CDF and its trigger requirements. In this, we have been guided by discussions with several of our experimental colleagues.

At this point, we emphasize that we have made no attempt to analyze real data or to put any mass limits on $\widetilde{W}$ and $\widetilde{Z}$ masses. We believe that this is an experimental question. Rather, it is the purpose of this paper to analyze the possible signals that would result if $\widetilde{W}$ and $\widetilde{Z}$ were light enough to be produced at present energies, or to indicate the mass limits that may be attainable should an absence of any signal be conclusively established. The extent to which attainable mass limits may be improved due to the higher energy available at the Fermilab Tevatron has also been discussed.

Our main results are given in Secs. V–VII (for $v'/v=1$) and in Sec. IX (for the case of a light scalar neutrino). We first review the case $v'/v=1$, assuming the scalar fermions are all heavier than the gauginos. The corresponding situation for light scalar fermions has already been studied in Ref. 16. A variety of n jet + m lepton + $\not{p}_T$ signals result from the decays of $\widetilde{W}$ and $\widetilde{Z}$.

The hadronic decay of the gauginos leads to monojet and dijet + $\not{p}_T$ signals. We see from Fig. 8 that if we require a cross section of 30 pb for monojets (corresponding to about 20 events in the current UA1 data sample), a $\widetilde{W}$ ($\widetilde{Z}$) mass of 44 GeV (48 GeV) can be probed if $m_{\widetilde{\gamma}} \simeq 8$ GeV; the precise value of $m_{\widetilde{Z}}$ for a given $\widetilde{W}$ mass depends on $m_{\widetilde{\gamma}}$. The requirement of a 30-pb cross section at the Fermilab Tevatron enables one to probe $\widetilde{W}$ and $\widetilde{Z}$ masses of 58 and 63 GeV, respectively. From Fig. 9, the corresponding number of dijet + $\not{p}_T$ events can also be read off. For example, at CERN, the 20 monojet events discussed above should be accompanied by about 8 dijet events if gauginos are the source of the missing-energy events. We remind the reader that the number of monojet and dijet events discussed in this paragraph count only those events from the hadronic decay of both gauginos. In addition, there will be a contribution to these topologies from the mixed signals discussed in Sec. VII when a lepton from the decay of one of the gauginos is outside its acceptance or is misidentified as a hadron. This contribution, which will be discussed shortly must be added to the jet(s) $+$ $\not{p}_T$ signals from just the hadronic decays of the gauginos.

At this point, we once again warn the reader that the monojet and dijet events have substantial standard-model backgrounds.[47] These must be thoroughly understood before any signal can be claimed. Absence of a sufficient number of missing-p_T events would, however, lead to limits on the gaugino masses.

The leptonic decays of both gauginos lead to a series of spectacular trilepton and acollinear dilepton events with both like- and unlike-sign dileptons. These events all have substantial $\not{p}_T$ as can be seen from Figs. 20, 21, 23, and 24 and have very limited hadronic activity—only that resulting from initial-state QCD radiation. We believe that these events have very little standard-model background (see Baer *et al.*, Ref. 15) and that an observation of even a handful of such events would be a signal of new physics. We see from Fig. 16 that at $\sqrt{s}=630$ GeV about eight trilepton events are expected in the current UA1 data sample even for $m_{\widetilde{W}}=38$ GeV ($m_{\widetilde{Z}}=44$ GeV), i.e., right up to the phase space for $W\to\widetilde{W}\widetilde{Z}$. This assumes 100% detection efficiency for leptons within the acceptance. At Tevatron energies, for $m_{\widetilde{W}}=38$ GeV more than 20 trilepton events would be expected with the same amount of integrated luminosity. At both the CERN collider and the Fermilab Tevatron over half of these are expected to be trimuons. We believe that even if detection efficiencies are taken into account (see Sec. VI) enough events would survive to serve as a signal of new physics, particularly since these *must* be accompanied by acollinear like- and unlike-sign $\mu\mu$, $e\mu$, and ee events which we now discuss. Again for $m_{\widetilde{W}}=38$ GeV, we can read off from Figs. 17—19 that 15—20 dilepton $+$ $\not{p}_T$ events are expected in the present UA1 data, about a quarter of which contain same-sign dileptons. At the Tevatron, for the same $\widetilde{W}$ mass and integrated luminosity about 50 dilepton events may be anticipated, with one-fifth of them being same-sign dileptons. However, since many of these events contain muons, and because the muon detector at the CDF is not expected to be operating during the initial phase of Tevatron operation, we are not in a position to discuss the improvement due to the higher beam energy available. Our results illustrate the importance of muon detection and also the detection of electrons down to lower values of p_T.

In addition to the jet(s) $+$ $\not{p}_T$ and multilepton $+$ $\not{p}_T$ events discussed above, gaugino production would also lead to jet(s) $+$ lepton(s) $+$ $\not{p}_T$ events. We see from Fig. 25 that the largest signal at the CERN collider from these mixed decay modes is classified as monojets. Almost ten additional monojet events are expected in the current data sample. In addition, a handful of 1 $\mu+1$ jet and 1 $e+1$ jet events are expected. At the Tevatron, in addition to the monojets, there is a cross section of ≈ 75 pb for multilepton $+$ 1 jet and dimuon events accompanied by hadronic activity. Although these events are not as distinctive as those from purely leptonic decays of gauginos (in that there are large standard-model backgrounds from heavy-flavor production[49]) they must be present in a data sample along with spectacular multilepton and monojet (dijet) events if a gaugino signal is to be claimed.

If the decays $W\to\widetilde{W}\widetilde{Z}$ and $Z^0\to\widetilde{W}\overline{\widetilde{W}}$ are kinematically inaccessible, gaugino production would occur only via $W\to\widetilde{W}\widetilde{\gamma}$. This would lead to jet(s) $+$ $\not{p}_T$ signals already discussed and to single lepton $+$ $\not{p}_T$ signals shown in Fig. 26. It is clear that the lepton signal is swamped by the standard-model background, and hence, it appears that CERN LEP II would be much better suited for detecting $\widetilde{W}$ with masses exceeding $M_Z/2$ (Refs. 43, 28, and 7).

We have relaxed the condition $v'/v=1$ in Sec. IX. If this ratio is less than unity, it is possible for the scalar neutrino to be light with the other scalar fermions quite heavy [see Eq. (2.18)]. This ratio cannot be arbitrarily small since the $\widetilde{u}_L$ and $\widetilde{W}$ (Ref. 28) masses would then have been small enough for them to have been detected at e^+e^- colliders. For illustrative purposes, we have taken this ratio to be 0.5. In this case, the decay $W\to\widetilde{W}\widetilde{Z}$ leads to single-lepton signals which have large standard-model backgrounds and so the characteristic signature comes only from the $Z^0\to\widetilde{W}\overline{\widetilde{W}}$ with the $\widetilde{W}$ dominantly decaying via the two-body mode $\widetilde{W}\to l\widetilde{\nu}$. Since the hadronic decay modes are suppressed this leads to the large dilepton $+$ $\not{p}_T$ signal as shown in Fig. 27. It is interesting to note that because of the light scalar neutrino many more electrons pass the cuts as compared to the $v'=v$ case shown in Figs. 18 and 19. Even at CERN energies, the dilepton $+$ $\not{p}_T$ cross section is ~ 50 pb for $m_{\widetilde{W}}$ as large as 45 GeV which corresponds to over 30 acollinear dilepton events in the present data sample (modulo efficiency corrections).

In summary, we have examined the different signatures arising from the decays $W\to\widetilde{W}\widetilde{\gamma}$, $W\to\widetilde{W}\widetilde{Z}$, and $Z^0\to\widetilde{W}\overline{\widetilde{W}}$. For the case $v'/v=1$, we have shown that the hadronic decays of the gauginos lead to substantial rates for monojet and dijet events at both the CERN collider and Fermilab Tevatron. If the decays $W\to\widetilde{W}\widetilde{Z}$ and $Z^0\to\widetilde{W}\overline{\widetilde{W}}$ are kinematically accessible (this is consistent with experimental data as can be seen from Fig. 5) these events must be accompanied by a variety of spectacular multilepton events that are essentially free from the standard-model background. In addition, there would be an observable rate for jet(s) $+$ lepton(s) $+$ $\not{p}_T$ events. Absence of these signals in the accumulated data sample obtained at the CERN collider already implies that the decay $W\to\widetilde{W}\widetilde{Z}$ is kinematically suppressed, and thus $m_{\widetilde{W}}>36$—38 GeV corresponding to $m_{\widetilde{Z}}>42$—44 GeV depending on the photino mass (assumed to be $\lesssim 10$ GeV). Gauginos of masses at the above lower limits should give over 20 monojet events, about 8 trilepton and 15—20 dilepton $+$ $\not{p}_T$ events in the accumulated UA1 data sample which even after efficiency corrections should leave an observable signal. We further note that the recently announced[48] bound, $m_L > 41$ GeV, on the sequential lepton mass translates to a limit on $m_{\tilde{W}}$. If we require that the cross section for $\not{p}_T$ events from gauginos be less than the corresponding cross section from heavy leptons with $m_L = 41$ GeV, we find $m_{\tilde{W}} \gtrsim 40$ GeV (from monojets alone) and $m_{\tilde{W}} \gtrsim 44$ GeV (if we combine the signals in Figs. 8, 9, and 25). If the scalar neutrino is light (and the other scalar fermions heavy), the large rate for acollinear dilepton events may make it possible for the UA1 Collaboration to put a lower mass limit on the $\tilde{W}$ as high as 45 GeV. We note that these are direct mass limits and are, unlike the ASP limits,[10] independent of the scalar-fermion mass. With the increased luminosity available at the Fermilab Tevatron or with the inception of the new antiproton accumulator at CERN, even better limits may be possible.

ACKNOWLEDGMENTS

We thank R. Arnowitt, V. Barger, D. Cline, E. Duchovni, K. Kondo, P. Nath, W. Summers, J. Yoh, and D. Zeppenfeld for fruitful conversations. This work was done when one of the authors (K.H.) was at DESY. He wishes to thank R. D. Peccei and other members of the DESY theory group for their hospitality. This research was supported in part by the University of Wisconsin Research Committee with funds granted by the Wisconsin Alumni Research Foundation, and in part by the U.S. Department of Energy under Contract No. DE-AC02-76ER00881.

APPENDIX A: WEYL-BASIS CALCULATION OF THE HELICITY AMPLITUDES

In this appendix we present a self-contained review of the helicity-amplitude calculus of Ref. 26 which we used to obtain the formulas listed in Appendix B.

In order to get the formulas which allow fast numerical evaluation, we use the chiral representation of Dirac matrices and go to a two component notation. A four spinor ψ $[=u(p,\lambda)$ or $v(p,\lambda)]$ is given by

$$\psi = \begin{bmatrix} \psi_- \\ \psi_+ \end{bmatrix}, \quad \bar{\psi} = (\psi_+^\dagger, \psi_-^\dagger) \tag{A1}$$

with

$$u(p,\lambda)_\pm = \omega_{\pm\lambda}(p) \chi_\lambda(p) , \tag{A2a}$$

$$v(p,\lambda)_\pm = \pm\lambda\omega_{\mp\lambda}(p)\chi_{-\lambda}(p) . \tag{A2b}$$

Here λ is two times the helicity of the on-shell fermion or antifermion of momentum $p^\mu = (E, p_x, p_y, p_z)$, i.e., $\lambda = \pm 1$,

$$\omega_\pm(p) = (E \pm |\mathbf{p}|)^{1/2} , \tag{A3}$$

and $\chi_\lambda(p)$ is a normalized helicity eigenspinor expressed explicitly in terms of the particle three momentum as

$$\chi_+(p) = [2|\mathbf{p}|(|\mathbf{p}|+p_z)]^{-1/2} \begin{bmatrix} |\mathbf{p}|+p_z \\ p_x + ip_y \end{bmatrix} , \tag{A4a}$$

$$\chi_-(p) = [2|\mathbf{p}|(|\mathbf{p}|+p_z)]^{-1/2} \begin{bmatrix} -p_x + ip_y \\ |\mathbf{p}|+p_z \end{bmatrix} . \tag{A4b}$$

In the chiral representation, we have explicitly

$$\gamma^\mu = \begin{bmatrix} 0 & \sigma_+^\mu \\ \sigma_-^\mu & 0 \end{bmatrix} , \tag{A5}$$

$$\gamma^5 = \begin{bmatrix} -1 & 0 \\ 0 & 1 \end{bmatrix} , \tag{A6}$$

with the 2×2 matrix four-vectors

$$\sigma_\pm^\mu = (1, \pm\boldsymbol{\sigma}) \tag{A7}$$

expressed in terms of the Pauli matrices $\boldsymbol{\sigma} = (\sigma_x, \sigma_y, \sigma_z)$. It is easy to verify that the free spinors (A2) satisfy the Dirac equation

$$(\not{p})_\pm u(p,\lambda)_\pm = mu(p,\lambda)_\mp , \tag{A8a}$$

$$(\not{p})_\pm v(p,\lambda)_\pm = -mv(p,\lambda)_\mp , \tag{A8b}$$

and the convention

$$v(p,\lambda) = C\bar{u}^{\,T}(p,\lambda) , \tag{A9}$$

with $C = i\gamma^2\gamma^0$.

By inserting these explicit expressions into an arbitrary amplitude written in the four-spinor basis, one obtains easily the expression in the two-spinor basis. A contraction of Lorentz indices can now be performed by using the Fierz identities

$$(\sigma_\pm^\mu)_{ij}(\sigma_{\mp\mu})_{kl} = 2\delta_{il}\delta_{kj} , \tag{A10a}$$

$$(\sigma_\pm^\mu)_{ij}(\sigma_{\pm\mu})_{kl} = 2(\delta_{ij}\delta_{kl} - \delta_{il}\delta_{kj}) , \tag{A10b}$$

where the spinorial indices i, j, k, and l take the values 1 and 2. After making this contraction, one finds that our production (Sec. III) and decay (Sec. IV) amplitudes can be expressed entirely in terms of the basic spinorial product

$$T(p,q)_{\lambda\sigma} = \chi_\lambda^\dagger(p)\chi_\sigma(q) , \tag{A11}$$

which is just a complex number. We may regard this quantity as analogous to the basic dot products of vector calculus. Since all the helicity eigenspinors are expressed explicitly in terms of their three-momentum components in Eq. (A4), it is straightforward to evaluate the spinorial product $T(p,q)_{\lambda\sigma}$ as a function of two three-momenta and two helicity indices λ and σ. The matrix functions $T_{\lambda\sigma}(p,q)$ are not all independent. They satisfy

$$T(p,q)_{\lambda\sigma} = \lambda\sigma T(p,q)^*_{-\lambda,-\sigma} \tag{A12a}$$

and

$$T(p,q)_{\lambda\sigma} = T(q,p)^*_{\sigma,\lambda} . \tag{A12b}$$

All our helicity amplitudes are then expressed in terms of coupling constants, factors $\omega_\pm(p)$ of (A3) and the product T as defined by Eq. (A11). Numerical evaluation of each helicity amplitude is then straightforward. The full amplitudes are obtained by multiplying the production and decay amplitudes and then summing over intermediate particle helicities in the zero-width approximation for the decaying particles. Polarization-blind cross sections can then be obtained by summing the absolute value squared of each helicity amplitude over all the external particle helicities and averaging over the initial-particle helicities.

One advantage of the formalism of Ref. 26 is that all amplitudes are expressed in arbitrary Lorentz frame since no specification of the frame is made in defining the spinors, see Eqs. (A1)—(A4). Because each helicity amplitude transforms nontrivially under a Lorentz boost, the boost invariance of the polarization-summed squared amplitudes can serve as a nontrivial check of the numerical program.

APPENDIX B: LIST OF HELICITY AMPLITUDES

In this appendix, we present all the production and decay amplitudes appearing in our analysis in the standard form of Ref. 26, in terms of the quantities $\omega_\lambda(p)$ of Eq. (A3) and $T(p,q)_{\lambda\sigma}$ of Eq. (A11). Once one has set up routines to evaluate these as functions of four-momenta and helicity indices, it is straightforward to numerically evaluate all the expressions.

For simplicity, we have ignored quark and lepton masses in the expressions listed below. In this case, the quantity $\omega_\lambda(k)$ simplifies to

$$\omega_\lambda(p)=\delta_{\lambda,+}(2p^0)^{1/2} \quad \text{for } m=0 \ , \tag{B1}$$

which saves the helicity summation for light fermions.

The production amplitudes listed in Eq. (3.3) can be expressed as

$$\mathcal{M}_{\rm a}=\delta_{\sigma,-}\delta_{\bar\sigma,+}\sum_\alpha g_-^{udW} g_\alpha^{\tilde W\tilde V W} D_W(q+\bar q)T_1^\alpha \ , \tag{B2a}$$

$$\mathcal{M}_{\rm b}=-\delta_{\sigma,-}\delta_{\bar\sigma,+} g_-^{u\tilde W\tilde d} g_-^{\tilde V d\tilde d} D_{\tilde d_L}(q-p_2)T_2^- \ , \tag{B2b}$$

$$\mathcal{M}_{\rm c}=\delta_{\sigma,-}\delta_{\bar\sigma,+} g_-^{u\tilde V\tilde u} g_-^{\tilde W d\tilde u} D_{\tilde u_L}(q-p_1)T_3^- \ , \tag{B2c}$$

$$\mathcal{M}_{\rm d}=\delta_{\bar\sigma,-\sigma}\sum_\alpha\sum_V g_\sigma^{qqV} g_\alpha^{\tilde W\tilde W V} D_V(q+\bar q)T_1^\alpha \ , \tag{B2d}$$

$$\mathcal{M}_{\rm e}=-\delta_{\sigma,-}\delta_{\bar\sigma,+} g_-^{u\tilde W\tilde d} g_-^{\tilde W u\tilde d} D_{\tilde d_L}(q-p_2)T_2^- \ , \tag{B2e}$$

$$\mathcal{M}_{\rm f}=\delta_{\sigma,-}\delta_{\bar\sigma,+} g_-^{d\tilde W\tilde u} g_-^{\tilde W d\tilde u} D_{\tilde u_L}(q-p_1)T_3^- \ , \tag{B2f}$$

$$\mathcal{M}_{\rm g}=-\delta_{\bar\sigma,-\sigma} g_\sigma^{q\tilde Z\tilde q} g_\sigma^{\tilde V q\tilde q} D_{\tilde q_\sigma}(q-p_2)T_2^\sigma \ , \tag{B2g}$$

$$\mathcal{M}_{\rm h}=\delta_{\bar\sigma,-\sigma} g_\sigma^{q\tilde V\tilde q} g_\sigma^{\tilde Z q\tilde q} D_{\tilde q_\sigma}(q-p_1)T_3^\sigma \ . \tag{B2h}$$

Here, the summation over α is $+$ and $-$, that over V is γ and Z, and we use the notation $\tilde f_+$ and $\tilde f_-$ for $\tilde f_R$ and $\tilde f_L$, respectively. The terms T_i^α are expressed as

$$T_1^\alpha=4\alpha s_2(q^0\bar q^0)^{1/2}\omega_{\alpha s_1}(p_1)\omega_{-\alpha s_2}(p_2)[(\delta_{\alpha,-\sigma}-\delta_{\alpha,\sigma})T(p_1,q)_{s_1,\sigma}T(\bar q,p_2)_{\sigma,-s_2}+\delta_{\alpha,\sigma}T(p_1,p_2)_{s_1,-s_2}T(\bar q,q)_{\sigma\sigma}] \ , \tag{B3a}$$

$$T_2^\alpha=2(q^0\bar q^0)^{1/2}\omega_{\alpha s_1}(p_1)\omega_{-\alpha s_2}(p_2)T(p_1,\bar q)_{s_1,-\alpha}T(p_2,q)_{s_2,\alpha} \ , \tag{B3b}$$

$$T_3^\alpha=2(q^0\bar q^0)^{1/2}\omega_{\alpha s_2}(p_2)\omega_{-\alpha s_1}(p_1)T(p_2,\bar q)_{s_2,-\alpha}T(p_1,q)_{s_1,\alpha} \ , \tag{B3c}$$

in terms of the spinorial product T defined in Eq. (A11).

The decay amplitudes of Eq. (4.4) read

$$\mathcal{M}_{\rm i}=\delta_{\lambda_2,-}\delta_{\lambda_3,+}\sum_\alpha g_\alpha^{\tilde\gamma\tilde W W} g_-^{du W} D_W(k_2+k_3)T_4^\alpha \ , \tag{B4a}$$

$$\mathcal{M}_{\rm j}=\delta_{\lambda_2,-}\delta_{\lambda_3,+} g_-^{d\tilde W\tilde u} g_-^{\tilde\gamma u\tilde u} D_{\tilde u_L}(k_1+k_3)T_5^- \ , \tag{B4b}$$

$$\mathcal{M}_{\rm k}=\delta_{\lambda_2,-}\delta_{\lambda_3,+} g_-^{\tilde W u\tilde d} g_-^{d\tilde\gamma\tilde d} D_{\tilde d_L}(k_1+k_2)T_6^- \ , \tag{B4c}$$

$$\mathcal{M}_{\rm l}=\delta_{\lambda_3,-\lambda_2} g_{\lambda_2}^{f\tilde Z\tilde f} g_{\lambda_2}^{\tilde\gamma f\tilde f} D_{\tilde f_{\lambda_2}}(k_1+k_3)T_5^{\lambda_2} \ , \tag{B4d}$$

$$\mathcal{M}_{\rm m}=\delta_{\lambda_3,-\lambda_2} g_{\lambda_2}^{\tilde Z f\tilde f} g_{\lambda_2}^{f\tilde\gamma\tilde f} D_{\tilde f_{\lambda_2}}(k_1+k_2)T_6^{\lambda_2} \ , \tag{B4e}$$

$$\mathcal{M}_{\rm n}=\delta_{\lambda_2,-}\delta_{\lambda_3,+}\sum_\alpha g_\alpha^{\tilde W\tilde Z W} g_-^{udW} D_W(k_2+k_3)T_4^\alpha \ , \tag{B4f}$$

$$\mathcal{M}_{\rm o}=\delta_{\lambda_2,-}\delta_{\lambda_3,+} g_-^{u\tilde Z\tilde u} g_-^{\tilde W d\tilde u} D_{\tilde u_L}(k_1+k_3)T_5^- \ , \tag{B4g}$$

$$\mathcal{M}_{\rm p}=\delta_{\lambda_2,-}\delta_{\lambda_3,+} g_-^{\tilde Z d\tilde d} g_-^{u\tilde W\tilde d} D_{\tilde d_L}(k_1+k_2)T_6^- \ , \tag{B4h}$$

where

$$T_4^\alpha=4(k_2^0k_3^0)^{1/2}\omega_{\alpha\lambda_1}(k_1)\omega_{\alpha s}(p)[(\delta_{\alpha,+}-\delta_{\alpha,-})T(k_1,k_3)_{\lambda_1,-}T(k_2,p)_{-,s}+\delta_{\alpha,-}T(k_1,p)_{\lambda_1,s}T(k_2,k_3)_{--}] \ , \tag{B5a}$$

$$T_5^\alpha=2(k_2^0k_3^0)^{1/2}\omega_{-\alpha s}(p)\omega_{-\alpha\lambda_1}(k_1)T(k_2,p)_{\alpha,s}T(k_1,k_3)_{\lambda_1,\alpha} \ , \tag{B5b}$$

$$T_6^\alpha=2\alpha\lambda_1(k_2^0k_3^0)^{1/2}\omega_{\alpha s}(p)\omega_{\alpha\lambda_1}(k_1)T(k_3,p)_{-\alpha,s}T(k_2,k_1)_{\alpha,-\lambda_1} \ . \tag{B5c}$$

This completes the compilation of all the amplitudes. Since all the couplings are listed in Eq. (3.9) and the factors T_i^α are expressed in terms of $\omega_\alpha(p)$ [see Eq. (A3)] and $T(p,q)_{\alpha\beta}$ [see Eqs. (A4) and (A11)], it is now straightforward to numerically evaluate all of the amplitudes.

---

[1]For a review see, e.g., P. Langacker, Phys. Rep. **72C**, 785 (1981).

[2]H. Georgi, H. Quinn, and S. Weinberg, Phys. Rev. Lett. **33**, 451 (1974).

[3]G. 't Hooft, *Recent Developments in Gauge Theories* (Plenum Press, New York, 1985), p. 135; S. Dimopoulos and H. Georgi, Nucl. Phys. **B193**, 150 (1981); N. Sakai, Z. Phys. C **11**, 153 (1981); E. Witten, Nucl. Phys. **B185**, 513 (1981).

[4]For an early review and references to the original literature, see, e.g., P. Fayet and S. Ferrara, Phys. Rep. **32**, 249 (1977).

[5]For a review and references to the original literature on supergravity, see P. van Nieuwenhuizen, Phys. Rep. **68**, 189 (1981).

[6]For recent developments in superstring theories, see, e.g., M. B. Green, in *Proceedings of the Twelfth International Symposium on Lepton and Photon Interactions at High Energies*, Kyoto, Japan, 1985, edited by M. Konuma and K. Takahashi (Research Institute for Fundamental Physics, Kyoto University, Kyoto, 1986).

[7]For recent reviews on phenomenological consequences of supersymmetries, see, e.g., H. E. Haber and G. L. Kane, Phys. Rep. **117**, 75 (1985); S. Dawson, E. Eichten, and C. Quigg, Phys. Rev. D **31**, 1581 (1985); H. Baer *et al.*, in CERN Yellow Report No. 86-02, 1986, edited by J. Ellis and R. Peccei.

[8]See, e.g., S. Komamiya, in *Proceedings of the Twelfth International Symposium on Lepton and Photon Interactions at High Energies* (Ref. 6).

[9]B. Adeva *et al.*, Phys. Rev. Lett. **53**, 1806 (1984); W. Bartel *et al.*, Phys. Lett. **146B**, 126 (1984); for a theoretical analysis, see, e.g., D. Dicus, S. Nandi, W. W. Repko, and X. Tata, Phys. Rev. D **29**, 1317 (1984); **30**, 1112 (1984).

[10]G. Bartha *et al.*, Phys. Rev. Lett. **56**, 685 (1986); see also E. Fernandez *et al.*, *ibid.* **54**, 1118 (1985); M. Davier, in Proceedings of the XIII International Conference on High Energy Physics, Berkeley, 1986, edited by S. Loken (World Scientific, Singapore, to be published).

[11]C. Rubbia, in *Proceedings of the Twelfth International Symposium on Lepton and Photon Interactions at High Energies* (Ref. 6).

[12]R. M. Barnett, H. E. Haber, and G. L. Kane, Nucl. Phys. **B267**, 625 (1986); E. Reya and D. P. Roy, Phys. Lett. **166B**, 223 (1986).

[13]K. Hagiwara, in *Quark Structure of Matter*, proceedings of the Strasbourg-Karlsruhe Conference, Strasbourg, France and Karlsruhe, West Germany, edited by M. Jacob and K. Winter (World Scientific, Singapore, 1986), p. 613. See also, G. Farrar, Phys. Rev. Lett. **53**, 1029 (1984).

[14]H. E. Haber, G. L. Kane, and M. Quiros, Phys. Lett. **160B**, 297 (1985).

[15]R. Barbieri, N. Cabibbo, L. Maiani, and S. Petrarca, Phys. Lett. **127B**, 458 (1983); R. Barnett, H. E. Haber, and K. Lackner, Phys. Rev. Lett. **51**, 176 (1983); Phys. Rev. D **29**, 1381 (1984); N. Cabibbo, L. Maiani, and S. Petrarca, Phys. Lett. **132B**, 195 (1983); H. Baer, J. Ellis, D. V. Nanopoulos, and X. Tata, *ibid.* **153B**, 265 (1985).

[16]H. Baer and X. Tata, Phys. Lett. **155B**, 278 (1985).

[17]I. I. Bigi and S. Rudaz, Phys. Lett. **153B**, 335 (1985); L. Hall and S. Raby, *ibid.* **153B**, 433 (1985); V. Barger, W.-Y. Keung, and R. J. N. Phillips, Phys. Rev. D **32**, 320 (1985); A. P. Contogouris, H. Tanaka, and S. D. P. Vlassopulos, McGill University Report No. 86-0130, 1985 (unpublished); H. Baer *et al.*, Phys. Lett. **161B**, 175 (1985); H. Baer and X. Tata, Phys. Lett. **167B**, 241 (1986).

[18]A. Chamseddine, R. Arnowitt, and P. Nath, Phys. Rev. Lett. **49**, 970 (1982); **50**, 232 (1983); R. Barbieri, S. Ferrara, and C. Savoy, Phys. Lett. **119B**, 343 (1982); L. Ibáñez, *ibid.* **118B**, 73 (1982); H. P. Nilles, M. Srednicki, and D. Wyler, *ibid.* **120B**, 346 (1983); J. Ellis, D. V. Nanopoulos, and K. Tamvakis, *ibid.* **121B**, 123 (1983); L. Hall, J. Lykken, and S. Weinberg, Phys. Rev. D **27**, 2359 (1983); L. Alvarez-Gaumé, J. Polchinski, and M. Wise, Nucl. Phys. **B221**, 495 (1983); E. Cremmer, P. Fayet, and L. Girardello, Phys. Lett. **122B**, 41 (1983); J. Lykken and F. Quevedo, Phys. Rev. D **29**, 293 (1984).

[19]For reviews of supergravity models, see H. P. Nilles, Phys. Rep. **110C**, 1 (1984); P. Nath, R. Arnowitt, and A. Chamseddine, *Applied $N=1$ Supergravity ICTP Series in Theoretical Physics* (World Scientific, Singapore, 1984), Vol. I.

[20]Chamseddine, Arnowitt, and Nath (Ref. 18); S. Weinberg, *ibid.* **50**, 387 (1983).

[21]J. Ellis, J. S. Hagelin, D. V. Nanopoulos, K. Olive, and M. Srednicki, Nucl. Phys. **238**, 453 (1984).

[22]P. Nath, R. Arnowitt, and A. Chamseddine, Phys. Lett. **129B**, 445 (1983); D. Dicus, S. Nandi, and X. Tata, *ibid.* **129B**, 451 (1983); V. Barger *et al.*, *ibid.* **131B**, 372 (1983); P. Fayet, *ibid.* **133B**, 363 (1983); D. Dicus, S. Nandi, W. W. Repko, and X. Tata, Phys. Rev. D **29**, 67 (1984); G. Altarelli *et al.*, Nucl. Phys. **B245**, 215 (1984); S. Gottlieb and T. Weiler, Phys. Rev. D **32**, 1119 (1985); R. M. Barnett and H. E. Haber, *ibid.* **31**, 85 (1985).

[23]A. Chamseddine, P. Nath, and R. Arnowitt, Phys. Lett. **174**, 399 (1986).

[24]H. Baer, K. Hagiwara, and X. Tata, Phys. Rev. Lett. **57**, 294 (1986); Argonne Report No. ANL-HEP-CP-86-25, 1986 (unpublished); Wisconsin Report No. MAD/PH/296, 1986 (unpublished).

[25]K. Inoue, A. Kakuto, H. Komatsu, and S. Takeshita, Prog. Theor. Phys. **67**, 1889 (1982); C. Kounnas, A. B. Lahanas, D. V. Nanopoulos, and M. Quiros, Phys. Lett. **132B**, 135 (1983); Nucl. Phys. **B236**, 438 (1984); L. E. Ibáñez and C. López, *ibid.* **B233**, 511 (1984); L. E. Ibáñez, C. López, and C. Muñoz, *ibid.* **B256**, 218 (1985); A. Bouquet, J. Kaplan, and C. A. Savoy, *ibid.* **B262**, 299 (1985).

[26]K. Hagiwara and D. Zeppenfeld, Nucl. Phys. **B274**, 1 (1986).

[27]L. Alvarez-Guamé, M. Claudson, and M. Wise, Nucl. Phys. **B207**, 96 (1982); L. Hall and K. Hinchliffe, Phys. Lett. **112B**, 351 (1982); G. Farrar and S. Weinberg, Phys. Rev. D **27**, 2732 (1983).

[28]J. Ellis, L. Ibáñez, and G. G. Ross, Nucl. Phys. **B221**, 29 (1983), Nath, Arnowitt, and Chamseddine (Ref. 22); J. Ellis *et al.*, Phys. Lett. **132B**, 436 (1983); B. Grinstein, J. Polchinski, and M. Wise, *ibid.* **130B**, 285 (1983); Dawson, Eichten, and Quigg (Ref. 7); Dicus, Nandi, and Tata (Ref. 22); Haber and Kane (Ref. 7); A. Bartl, H. Fraas, and W. Majerotto, Z. Phys. C **30**, 441 (1986); H. Komatsu and J. Kubo, Nucl. Phys. **B263**, 265 (1986); X. Tata and D. A. Dicus, Phys. Rev. D (to

be published); our discussion closely parallels that of Tata and Dicus.

[29]G. Arnison *et al.*, Phys. Lett. **147B**, 493 (1984).

[30]Chamseddine, Arnowitt, and Nath (Ref. 18); Barbieri, Ferrara, and Savoy (Ref. 18).

[31]These models contain an extra singlet Higgs field U that gives off-diagonal mass terms with h^0 and $h^{0\prime}$. Such models appear to have problems with radiative corrections and need either the introduction of a pair of extra doublets or the choice of other representations of the grand unification group for their stability (see Ref. 32).

[32]S. Ferrara, D. V. Nanopoulos, and C. A. Savoy, Phys. Lett. **123B**, 214 (1983).

[33]P. Nath, R. Arnowitt, and A. Chamseddine, Harvard Report No. HUTP-83-A077, 1983 (unpublished).

[34]L. J. Hall and J. Polchinski, Phys. Lett. **152B**, 335 (1985).

[35]R. M. Barnett, H. E. Haber, and K. S. Lackner, Phys. Lett. **126B**, 64 (1983); Phys. Rev. D **29**, 1990 (1984).

[36]J. S. Hagelin, G. L. Kane, and S. Raby, Nucl. Phys. **B247**, 638 (1984); L. E. Ibáñez, Phys. Lett. **137B**, 160 (1984).

[37]D. W. Duke and J. F. Owens, Phys. Rev. D **30**, 49 (1984).

[38]V. Barger, R. Robinett, W.-Y. Keung, and R. J. N. Phillips, Phys. Rev. D **28**, 2912 (1983); see also D. Dicus *et al.*, Phys. Rev. Lett. **51**, 1030 (1983).

[39]L. DiLella, in *Proceedings of the Twelfth International Symposium on Lepton and Photon Interactions at High Energies* (Ref. 6), p. 280.

[40]F. Halzen and K. Mursula, Phys. Rev. Lett. **51**, 857 (1983); K. Hikasa, Phys. Rev. D **29**, 1939 (1984); N. G. Deshpande, G. Eilam, V. Barger, and F. Halzen, Phys. Rev. Lett. **54**, 1757 (1985).

[41]The value of R was calculated for gauge boson decays into gauginos by Chamseddine, Nath, and Arnowitt (Ref. 23); see also N. Deshpande, in *New Particles '85*, proceedings of the Conference, Madison, Wisconsin, 1985, edited by V. Barger, D. Cline, and F. Halzen (World Scientific, Singapore, 1986).

[42]UA1 Collaboration, J. Rohlf, Report No. CERN-EP/85-160, 1985 (unpublished); C. Rubbia, in *Proceedings of the Twelfth International Symposium on Lepton and Photon Interactions at High Energies* (Ref. 6).

[43]T. Schimert, C. Burgess, and X. Tata, Phys. Rev. D **32**, 707 (1985).

[44]See V. Barger *et al.*, Phys. Rev. D **29**, 887 (1984).

[45]J. Rohlf, in *Proceedings of the Oregon Meeting,* Annual Meeting of the Division of Particles and Fields of APS, Eugene, 1985, edited by R. Hwa (World Scientific, Singapore, 1986), p. 66.

[46]F. Halzen *et al.*, Z. Phys. C **14**, 351 (1982).

[47]S. Ellis, R. Kleiss, and W. J. Stirling, Phys. Lett. **158B**, 341 (1985); **167B**, 464 (1986); J. R. Cudell, F. Halzen, and K. Hikasa, *ibid.* **157B**, 447 (1985); P. Aurenche and R. Kinnunen, Z. Phys. C **28**, 261 (1985); R. Odorico, Phys. Rev. D **32**, 3055 (1985); **33**, 2711 (1986); E. W. N. Glover and A. D. Martin, Z. Phys. C **29**, 399 (1985); V. Barger, J. Ohnemus, and R. J. N. Phillips, Phys. Rev. D **35**, 158 (1987).

[48]A. Honma, in Proceedings of the XIII International Conference on High Energy Physics, Berkeley, California, 1986 (Ref. 10).

[49]For an overview, see, e.g., R. J. N. Phillips, in *New Particles 1985,* edited by V. Barger, D. Cline, and F. Halzen (World Scientific, Singapore, 1986), and references cited therein.

[50]Note that for the CDF detector, we required $|\eta_\mu| < 4.0$.

[51]D. Cline and C. Rubbia, Phys. Lett. **127B**, 277 (1983); Dicus, Nandi, Repko, and Tata (Ref. 22); V. Barger *et al.*, Phys. Lett. **127B**, 277 (1983); Phys. Rev. D **29**, 2020 (1984); S. Gottlieb and T. Weiler, Phys. Rev. D **29**, 2005 (1984).

[52]Baer *et al.* (Ref. 17).

[53]Tata and Dicus (Ref. 28).

[54]Admittedly, for nonzero values of $m_{\tilde{\gamma}}$, it is possible to choose $v'/v > 1$ so that $\tilde{W} \rightarrow \tilde{l}_L \bar{\nu}$ is the dominant decay mode. We would have to ensure $m_{\tilde{l}_L} \gtrsim 23$ GeV. We have not studied this possibility in detail in this paper, but it is straightforward to do so.